Supporting Information

Toward Efficient Tandem Electroreduction of CO_2 to Methanol using Anodized Titanium

Wei Jie Teh[a], *Oriol Piqué*[b], *Qi Hang Low*[a], *Weihan Zhu*[a], *Federico Calle-Vallejo*[b,*], *Boon Siang Yeo*[a,*]

[a] Department of Chemistry, National University of Singapore, 3 Science Drive 3, Singapore 117543 and Solar Energy Research Institute of Singapore, National University of Singapore, 7 Engineering Drive 1, Singapore 117574.

[b] Department of Materials Science and Chemical Physics & Institute of Theoretical and Computational Chemistry (IQTCUB), University of Barcelona, Martí i Franquès 1, 08028 Barcelona, Spain.

* To whom correspondence should be addressed: BSY (Email: chmyeos@nus.edu.sg) or FCV (Email: f.calle.vallejo@ub.edu).

Contents

S1. Experimental and computational methods

S1.1. Anodization of Ti substrate

A polycrystalline titanium disc (99.99%, Diameter: 15 mm, Goodfellow) was progressively polished using a SiC paper (Grit 1200, Struers), 15- and 3 μm diamond slurries (Diapro, Struers). The disc was then sonicated in ultrapure water (18 MΩ) to remove any residual diamond slurry. The polished Ti disc was anodized in 0.2 M KCl electrolyte (99.0%, Sigma-Aldrich) at 0.25 A/cm^2 at 1, 2, 3 or 4 min. A platinum wire was used as counter electrode. The anodized Ti foil will be referred to as Ti_{an}. The exposed electrode area was 0.785 cm^2. An Autolab PGSTAT 30 potentiostat (Eco Chemie) was used for controlling the electrochemistry.

S1.2. Preparation of control samples

The performance of the Ti_{an} catalyst for formic acid reduction (FAR) to methanol was compared against those of a polished Ti disc (0.785 cm^2) and commercial TiO_2 samples. 20 mg of commercial rutile (Sigma Aldrich, 99.9%, < 5 μm) or anatase (Sigma Aldrich, 99.8%, < 5 μm) TiO_2 was sonicated with 25 μL of Nafion® (5 % in aliphatic alcohols, Sigma Aldrich), 250 μL of ethanol (VWR chemicals, 99.97%) and 725 μL of ultrapure water. 25 μL of the catalyst ink was then dropcast onto a polished Ti disc and dried under a heat lamp, before being used for electrolysis.

S1.3. Electrochemical reduction of formic acid

FAR was conducted in 0.5 M HCOOH (Fluka, 98.0–100%) dissolved in aqueous 0.1 M K_2SO_4 (99.99%, Meryer) supporting electrolyte. A three-electrode configuration was used, with Ag/AgCl (saturated KCl, Pine) and graphite (Ted Pella) as the reference and counter electrodes, respectively. The cathodic (12 mL of 0.1 M K_2SO_4 + 0.5 M HCOOH) and anodic (8 mL of 0.1 M K_2SO_4) compartments were separated by a cation exchange membrane (CMV, AGC Asahi Glass).

A potentiostat (Gamry reference 600) was used to control the electrolysis of formic acid using chronoamperometry (CA). The current interrupt mode was used to compensate for the iR drop during CA measurements. The electrolysis period was 60 min. The potentials in this work are referenced to the reversible hydrogen electrode (RHE) using the average potential of the Ag/AgCl electrode ($E_{Ag/AgCl}$) (Equation 1).

$$E_{RHE} = E_{Ag/AgCl} + 0.197 + (0.059 \cdot pH) \quad (1)$$

The gaseous products (H_2, CO, CH_4) were detected from the cathodic compartment by an on-line gas chromatograph (GC, Agilent 7890A) with flame ionization detectors (FIDs) and a thermal conductivity detector (TCD). N_2 (Chemgas, 99.999 %) was used as the carrier gas. The measurements were made over the course of seven GC injections (intervals of 492 s between adjacent injections). To ensure that the reported data is from a system under equilibrium conditions, only measurements obtained from the 4th to 7th injections were used for analyses. Details of our chromatography setups have been described in our previous work.[1] Solutions at various pH values (2.6, 3.4, 4.5 and 5.8) were adjusted with KOH (99.99%, Sigma-Aldrich) for 6 h electrolysis experiments. After electrolysis, the liquid products were analyzed using headspace-GC (HS-GC, Agilent, 7890B and 7697A). The sample was equilibrated in an oven at 90 ^{o}C for 30 min, before its headspace was injected into the GC. An example of the HS-GC chromatogram obtained is shown in Figure S4.

The presence of methanol was also verified using ^{1}H nuclear magnetic resonance spectroscopy. 1 mL of catholyte was mixed with 50 μL internal standard, which consisted of 25 mM phenol (99.5%, Scharlau) and 5 mM dimethyl sulfoxide (DMSO, 99.9%, Quality Reagent Chemical). 540 μL of this mixture was further mixed with 60 μL D_2O (99.96 % D, Cambridge Isotope Lab), and transferred to a NMR sample tube. ^{1}H NMR spectroscopy was performed with a 500 MHz spectrometer (Avance 500, Bruker). The water suppression method was used. The spectrum was collected after 16 continuous scans. An example of the ^{1}H NMR spectrum obtained is shown in Figure S4.

Formaldehyde (CH_2O) concentrations were measured using the chromotropic acid method.[2] 1 mL of electrolyte was added into a 10 mL volumetric flask, followed by 0.14 mL of 5 % chromotropic acid disodium dihydrate solution (technical grade, Sigma-Aldrich). 5 mL of concentrated sulfuric acid (98%, Fisher-Scientific) was then added, with the flask placed in a cool water bath. The solution was topped up to the mark using 0.1 M K_2SO_4, left to stand for 15 min, and then analyzed using a Shimadzu UV-3600 UV-Vis-NIR spectrometer.

S1.4. Electrochemical reduction of formaldehyde

A three-electrode cell was used, with a cation exchange membrane to separate the anodic and cathodic compartments. Ag/AgCl (saturated KCl) and graphite were respectively employed as the reference and counter electrodes. A nominal amount (5 mM) of CH_2O (16% v/v, methanol-free, Sigma-Aldrich) was added into 14 mL of 0.1 M K_2SO_4 electrolyte. Before

CH_2O electrolysis, 1 mL of solution was extracted for HS-GC analysis for CH_3OH detection, while another 1 mL was extracted for formate detection using high-performance liquid chromatography (Agilent, HPLC–1260 Infinity Series; Aminex HPX-87H column; variable wavelength detector, and 0.5 mM H_2SO_4 mobile phase). The quantification process was repeated after 60 min of CH_2O electrolysis. The amount of HCOOH and CH_3OH formed from Cannizzaro disproportionation is based on the difference in HCOOH and CH_3OH concentrations before and after CH_2O electrolysis.[3] The amount of CH_2O present in the electrolyte was quantified using the chromotropic acid method.

S1.5. Characterization of catalysts

Scanning Electron Microscopy (SEM) (JEOL JSM-6701F, 5 keV) was employed to characterise the surface morphologies of the catalysts.

X-ray diffraction (XRD) analysis was used to determine the composition of the catalyst. The system used was a Bruker D8 Advance (Cu K_α 40 kV, 40 mA) with 2D Lynxeye XE PSD Counter detector, with the incoming signal fixed at 5°. The samples were loaded on a low background Si wafer (Diffraction free, p-type doped B, KMT corporation).

X-ray photoelectron spectroscopy (XPS) was used to analyse the surface composition of the Ti electrodes. XPS measurements were performed using a SPECS system with XR50 X-ray Mg K_α (1253.7 eV) source. Surface etching was done by Ar ion sputtering with an operation energy of 2.0 kV under an argon pressure of 10^{-5} mbar. The adventitious C_{1s} peak at 285.0 eV was used as reference for calibrating the binding energies.

Raman spectroscopy was performed using a confocal Raman microscope (Horiba Jobin Yvon) in an epi-illumination mode (top-down). A He-Ne laser with 633 nm wavelength (CVI Melles Griot) was used as the excitation source. The laser beam was focused on the samples using a dry objective lens (×50 Olympus MPlan N, numerical aperture 0.75). The back-scattered light was filtered through a 633 nm edge filter, before being directed into a spectrograph (iHR320) / charge-coupled device detector (Synapse CCD). The acquisition time of each spectrum was 30 s.

Diffuse Reflectance Spectroscopy (DRS) was performed using a Shimadzu UV-3600 UV-Vis-NIR spectrometer. The samples were placed on the sample holder for analysis, with $BaSO_4$ powder (Wako) as the reference.

Electron Paramagnetic Resonance (EPR) Spectroscopy was performed using a JEOL FA200 ESR spectrometer. The Ti_{an} layers were removed from the Ti substrates, weighed, and loaded into a 250 mm Wilmad Quartz (Cfq) EPR (Diam. 5mm) tube for analysis. The spectra were measured at a microwave frequency of approximately 9.207 GHz, microwave power of 1.0 mW, modulation frequency of 100 kHz, width of 1.0 mT, sweep time of 2 min and time constant of 0.1 s. All spectra were taken at room temperature. Mn^{2+} embedded in MgO was used as a reference for all experimental g values. All signal areas were taken using the numerical double integration of the EPR spectra peaks.[4,5]

Cyclic voltammetry was conducted on the samples after FAR. The electrolyte used was 0.1 M K_2SO_4 + 0.5 M HCOOH. The working electrode was scanned from –1.25 to 1.35 V vs RHE, at a scan rate of 50 mV/s. The TOV anodic peak area was measured from –0.85 to 1.35 V vs RHE.

Elemental analysis of the catholyte before and after FAR was performed using a Perkin Elmer Avio 500 Inductively Coupled Plasma-Optical Emission Spectrometer (ICP-OES).

S1.6. Computational methods

The VASP code was used to perform the DFT simulations.[6] The PBE exchange-correlation functional was used to estimate the total energies[7] and the projector augmented wave method was used to describe ion-electron interactions.[8] To help in localizing the *d* states of Ti atoms, a Hubbard U_{eff} of 5 eV was used, obtained in previous works through a linear-response method.[9] We used a plane-wave cutoff of 450 eV, k_BT = 0.2 eV (extrapolating total energies to 0 K), and the conjugate-gradient optimization algorithm until the maximal force on any atom was below 0.05 eV/Å.

The optimized bulk parameters were found to be a = 2.995 Å and b = 4.715 Å for the rutile phase, and a = 3.889 Å and b = 9.732 Å for the anatase phase. All TiO_2 slab models had 4 atomic layers, the two bottommost were fixed at the bulk equilibrium distances, whereas the topmost two and the adsorbates were fully allowed to relax. The TiO_2(110) slab contained 24 Ti and 48 O atoms, the TiO_2(120)-CT and TiO_2(120)-BT slabs had 39 Ti and 78 O atoms each, and the A-TiO_2(101) slab had 32 Ti and 64 O atoms. Those slabs avoid lateral interactions between adsorbates. The vertical distance between repeated images was at least 13 Å. Monkhorst-Pack[10] meshes of 4×6×1, 3×4×1, 3×4×1, and 3×5×1 for TiO_2(110), TiO_2(120)-CT,

TiO_2(120)-BT, and A-TiO_2(101), respectively, ensured convergence of the adsorption energies within 0.05 eV. Isolated molecules were calculated in boxes of 9 Å × 10 Å × 11 Å using k_BT = 0.001 eV and sampling the Γ-point only.

The reaction free energies were approximated as $\Delta G \approx \Delta E_{DFT} + \Delta ZPE - T\Delta S$, where ΔE_{DFT} is the DFT-calculated reaction energy, ΔZPE is the zero-point energy change and $T\Delta S$ is the entropy change at T = 298.15 K. ΔS only includes vibrational contributions for the adsorbates and all contributions for the free molecules. No explicit solvation was considered for two reasons: (I) the scope of this work is the identification of activity trends which, according to previous studies, remain intact after the inclusion of explicit solvation in TiO_2.[11] (II) Our systems are large, and the inclusion of explicit solvation would make this work intractable. However, we did perform implicit solvent calculations for the intermediates in the most favorable pathways on TiO_2(110) and TiO_2(110)-O.[12] In general, we observed a destabilization of all adsorbates by ~0.3 eV, in agreement with previous theoretical works.[13] The results are shown in Section S1.9.

The energetics of proton-electron pairs was evaluated using the computational hydrogen electrode approach.[14] The limiting potentials U_L were calculated based on the largest positive free energies of reaction: $U_L = -\Delta G_{max}/e^-$, where e^- is the charge of an electron. To ensure that the calculated and experimental equilibrium potentials agree, we corrected the total energies of liquids and gases using a semiempirical method.[15]

S1.7. Gas-phase corrections

The free energies of gas-phase molecules were estimated as: $G = E_{DFT} + ZPE - TS$. ZPE values were obtained from vibration frequency analyses and TS values were obtained from thermodynamic tables at T = 298.15 K, see Table S1. Moreover, corrections to the formation energies of 0.19, 0.04, 0.03, and 0.46 eV were applied to HCOOH, CH_3OH, CH_4, and O_2, respectively, following the method described by Granda-Marulanda et al.[15]

Table S1. Zero-point energy and entropy contributions to the free energies of gas-phase molecules. All values are in eV.

Molecule	ZPE	TS
H_2	0.27	0.40
H_2O	0.57	0.58
O_2	0.10	0.63
CH_4	1.19	0.58
CH_3OH	1.34	0.74
HCOOH	0.89	0.77

S1.8. Liquid-phase corrections

Formic acid, methanol, and water are in the liquid phase. Their free energies from gas-phase DFT calculations are approximated using the method described by Calle-Vallejo et al.,[16] which is based on TS corrections. Such corrections are for formic acid, methanol, and water –0.13, –0.04, and –0.09 eV, respectively.

S1.9. Implicit solvent calculations

Table S2. Free energies of adsorption of the intermediates involved in the most favorable pathway of FAR to methanol, with implicit solvent (ΔG_{sol}), without it (ΔG), and their absolute difference ($\Delta\Delta G$). All values are in eV.

TiO_2(110)	ΔG	ΔG_{sol}	$\Delta\Delta G$
*HCOOH	–0.44	–0.05	0.38
*H_2COOH	1.27	1.76	0.49
*H_2CO	–0.09	0.28	0.37
*H_3CO	1.12	1.45	0.32

TiO_2(110)-O	ΔG	ΔG_{sol}	$\Delta\Delta G$
*HCOOH	–0.03	0.18	0.21
*H_2COOH	–1.11	–0.57	0.54
*O + $CH_3OH_{(l)}$	–1.64	–1.63	0.02
*OH	–1.58	–1.24	0.34

S2. Characterization of catalysts

S2.1. X-ray photoelectron spectroscopy of Ti_{an}

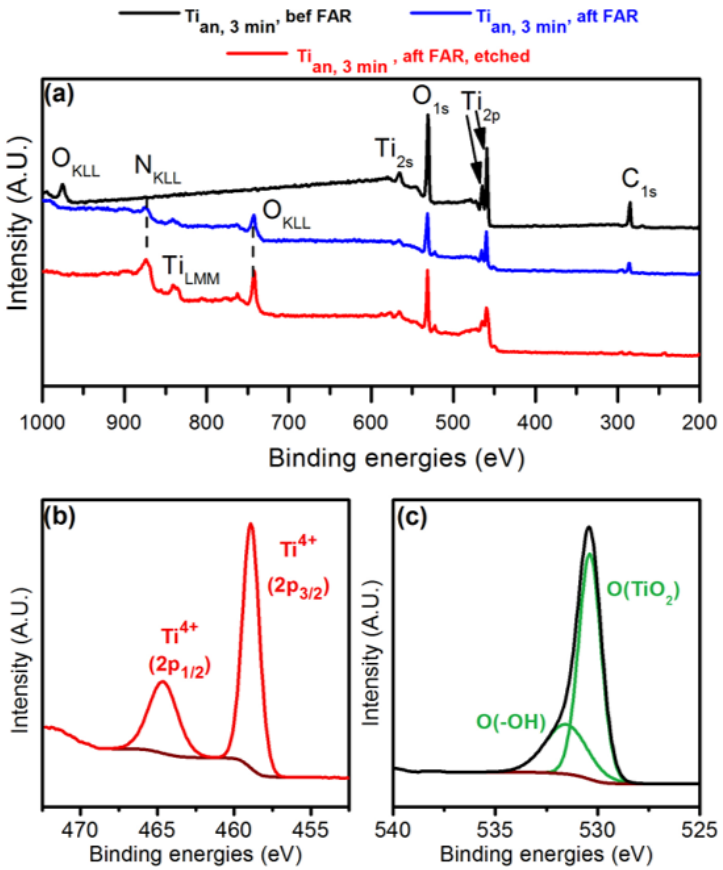

Figure S1. (a) XPS survey spectra of a $Ti_{an,\ 3\ min}$ catalyst before and after FAR at –1.00 V vs RHE. (b)-(c): Ti_{2p} and O_{1s} spectra of $Ti_{an,\ 3\ min}$ after FAR at –1.00 V vs RHE, before Ar^{+} etching.

Table S3. Experimental (Exp) and literature (Lit) O_{1s} binding energies (BEs) of lattice TiO_2 (Ti-O) and surface hydroxyl groups (Ti-OH) in different forms of TiO_2.

Ti-O BEs (eV) (Exp)	Ti-OH BEs (eV) (Exp)	TiO_2 substrate	Ti-O BEs (eV) (Lit)	Ti-OH BEs (eV) (Lit)	References
530.4	531.6	Amorphous	530.5	531.8	[17]
		Anatase	530.5	531.5	[18]
		Rutile	530.1	531.7	[19]

S2.2. Diffuse reflectance spectroscopy of Ti_{an} catalyst

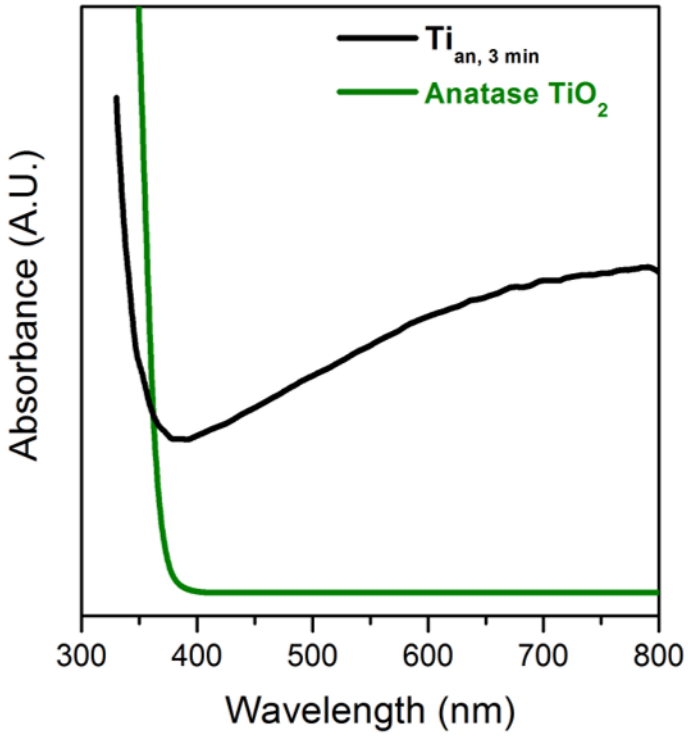

Figure S2. Diffuse reflectance spectroscopy (DRS) spectra of $Ti_{an,\ 3\ min}$ sample after FAR at –1.00 V vs RHE. For comparison, commercial anatase TiO_2 was also analyzed using DRS. The absorption region in the UV region (< 400 nm) is attributed to the 3.2 eV band gap transition in bulk TiO_2.[20] The absorption between 400 to 800 nm observed in the $Ti_{an,\ 3\ min}$ catalyst is attributed to TOVs, resulting in a continuous vacancy band of electronic states induced below the conduction band of TiO_2.[21]

S2.3. X-ray diffraction of Ti_{an} catalyst

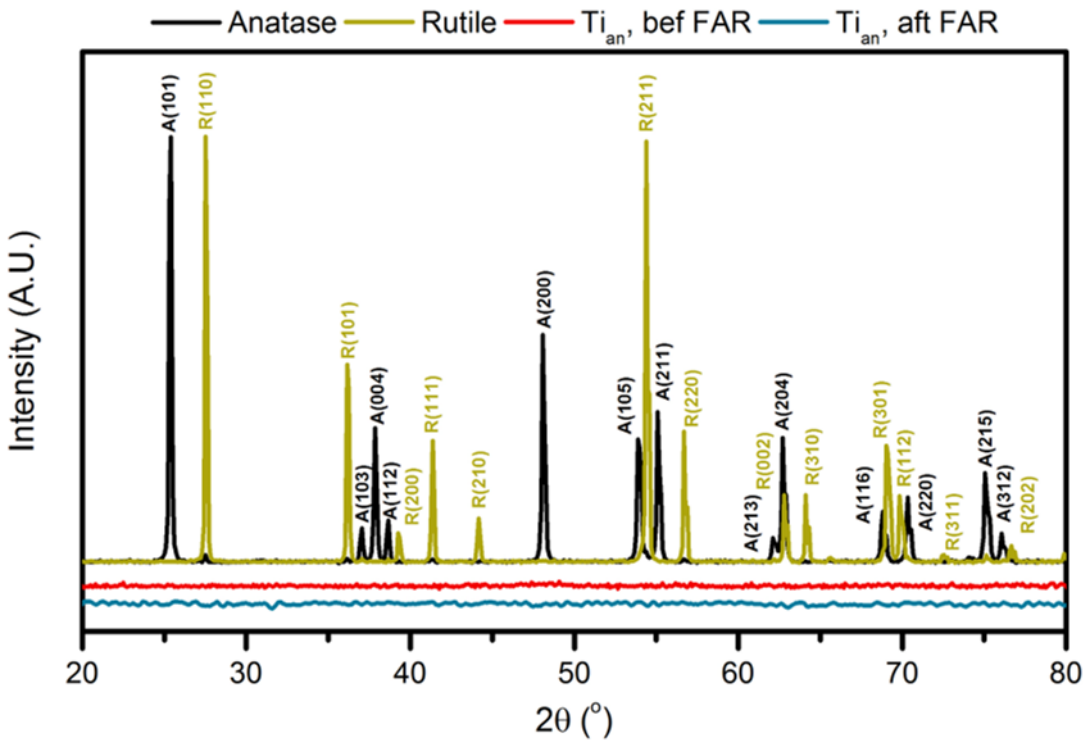

Figure S3. XRD analysis of $Ti_{an,\ 3\ min}$ powder before and after FAR at –1.00 V vs RHE. For comparison, crystalline anatase and rutile TiO_2 samples were also analyzed using XRD. No well-defined anatase or rutile TiO_2 XRD peaks were observed from the $Ti_{an,\ 3\ min}$ powder before and after FAR. This indicates that the anodized catalyst was XRD-amorphous.

S2.4. Raman spectroscopy of Ti_{an} catalyst

Table S4. Observed Raman shifts and peak assignments for titanium species shown in Figure 1g

Raman shift (cm^{-1}) of titanium species						
Ti_{an}, before electrolysis	Ti_{an}, after FAR electrolysis		Rutile TiO_2 standard	Anatase TiO_2 standard	Literature values	Peak assignment
	Major	Minor				
153	153	-	142	-	144	B_{1g} (Rutile)
-	-	-	236	-	235	Second-order Raman scattering
446	446	-	446	-	448	E_g (Rutile)
610	610	-	610	-	612	A_{1g} (Rutile)
-	-	151	-	142	147	E_g (Anatase)
-	-	398	-	398	398	B_{1g} (Anatase)
-	-	515	-	515	515	A_{1g}, B_{1g} (Anatase)
-	-	630	-	639	640	E_g (Anatase)

Literature values for rutile and anatase TiO_2 are taken from [22].

S3. Electrolysis on Ti_{an}

S3.1. Electrolysis of HCOOH on Ti_{an}

Table S5. Products obtained from the electrocatalytic FAR using $Ti_{an,\ 3\ min}$ catalysts at different applied potentials. Electrolysis were conducted for 60 min in 0.1 M K_2SO_4 + 0.5 M HCOOH.

Potential	**Products obtained**					**CH_3OH detected**
(V vs RHE)	CH_3OH	H_2	CH_4	CH_2O	Total	**(μM)**
–0.90	**8.4±1.9** *–1.07±0.29*	**77±10** *–9±4*	**1.7±0.9** *–0.15±0.04*	**0.41±0.07** *–0.019±0.003*	**87±11** *–10±4*	594±183
–0.95	**10.2±1.8** *–1.39±0.13*	**81±9** *–11±4*	**1.3±0.4** *–0.17±0.01*	**0.24±0.04** *–0.021±0.002*	**93±9** *–13±4*	771±135
–1.00	**12.6±1.8** *–1.95±0.20*	**77±3** *–12±2*	**1.4±0.3** *–0.20±0.03*	**0.14±0.04** *–0.019±0.001*	**91±4** *–14±2*	1122±188
–1.05	**5.3±1.0** *–1.96±0.19*	**88±8** *–29±7*	**0.8±0.2** *–0.23±0.05*	**0.06±0.01** *–0.024±0.005*	**94±8** *–31±7*	1231±93
No potential (pre-reduced Ti_{an})	N.D.	N.D.	N.D.	N.D.	-	N.D.

Numbers in bold are the Faradaic efficiencies in %, while numbers in italics are partial current densities in mA/cm^2. N.D.: Not detected.

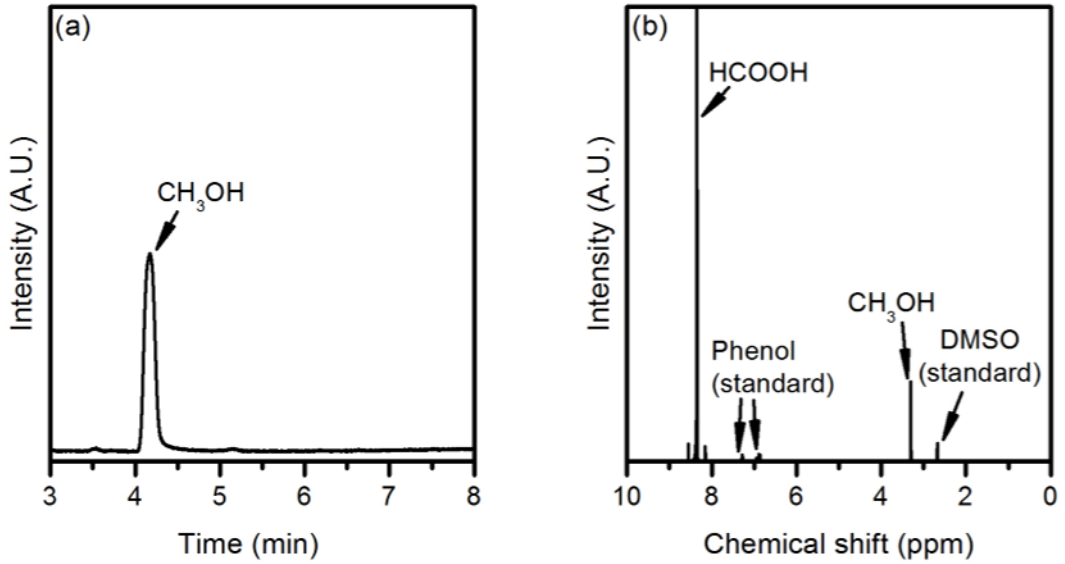

Figure S4. Detection of CH_3OH in the electrolyte using (a) HS-GC and (b) ^1H NMR. The electrolyte was analyzed after FAR, with FAR performed using $Ti_{an,\ 3\ min}$ catalysts biased at –1.00 V vs RHE.

S3.2. Electrolysis of FAR products on Ti_{an}

Table S6. Data obtained from the reduction of CH_3OH or CH_2O on a $Ti_{an,\ 3\ min}$ catalyst at –1.00 V vs RHE.

Reactant	Current density (mA/cm^2)	CH_4 detected (ppm)
CH_3OH	–5.1	N.D.
CH_2O	–1.9	N.D.

N.D.: Not detected.

S3.3. Production of CO from HCOOH

Table S7. Concentrations of CO detected from a $Ti_{an,\ 3\ min}$ catalyst in the presence of HCOOH.

Injection	CO detected (ppm)
	FAR, –1.00 V vs RHE
1	9.9
2	14.2
3	3.8
4	3.0
5	3.6
6	3.9
7	4.5

S3.4. Stability tests for FAR on Ti_{an}

Table S8. Stability test of $Ti_{an,\ 3\ min}$ at –1.00 V vs RHE for six hours. The electrolyte used was 0.1 M K_2SO_4 + 0.5 M HCOOH at pH 2.6.

Electrolyte pH	Time (h)	FE_{CH3OH} (%)	Accumulative CH_3OH concentrations (mM)
2.6	1	13.8 ± 1.3	0.8 ± 0.2
	2	11.3 ± 1.8	1.5 ± 0.3
	3	8.8 ± 2.5	2.1 ± 0.4
	4.5	4.9 ± 0.8	2.7 ± 0.6
	6	3.4 ± 1.6	3.2 ± 0.5

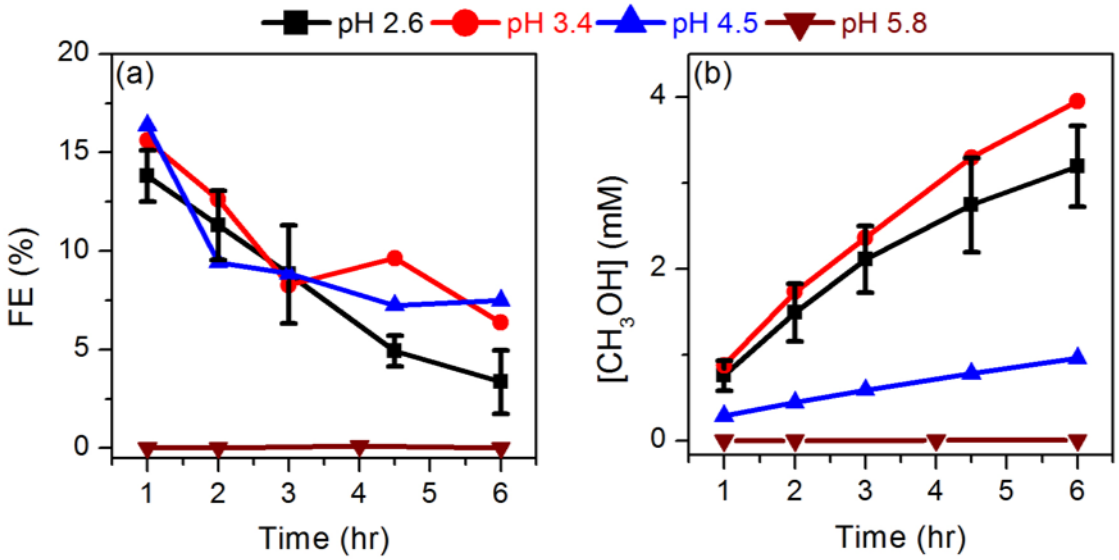

Figure S5. (a) Faradaic efficiencies (%) and (b) accumulated concentrations (mM) of CH_3OH after six hours FAR at –1.00 V vs RHE at various pH values. The pH values were adjusted using KOH.

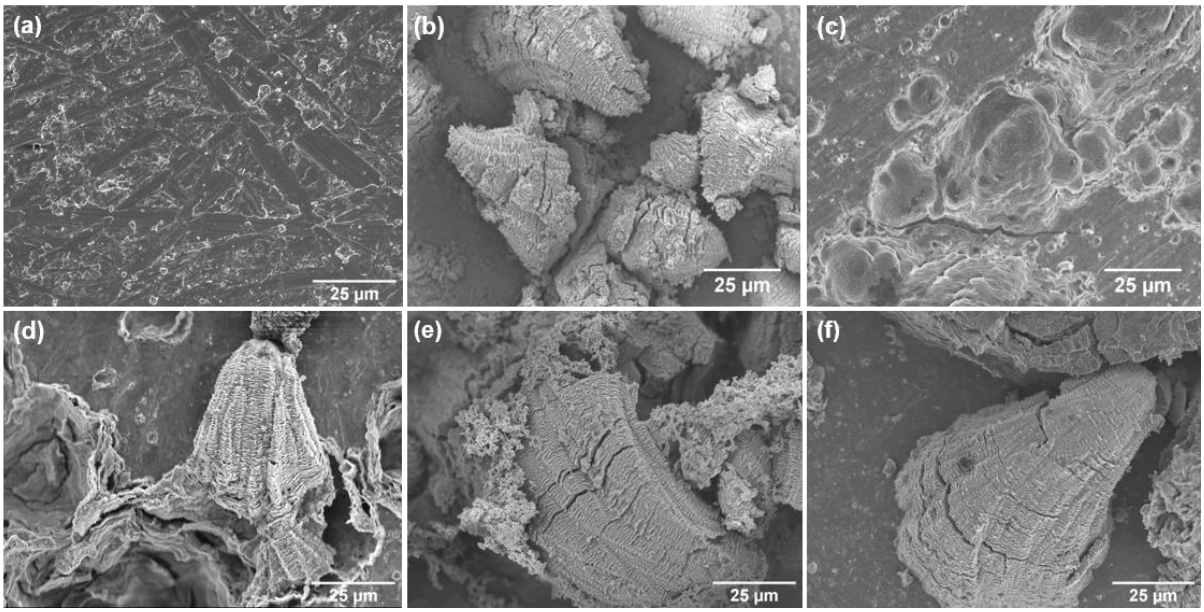

Figure S6. SEM images of (a) polished Ti disc, and (b) Ti disc anodized in 0.2 M KCl for 3 min ($Ti_{an,\ 3\ min}$), before FAR. $Ti_{an,\ 3\ min}$ after six hours of FAR at –1.00 V vs RHE at (c) pH 2.6, (d) pH 3.4, (e) pH 4.5, and (f) pH 5.8. Significant loss of $Ti_{an,\ 3\ min}$ catalyst was observed after six hours of FAR at pH 2.6, and the amount of delaminated $Ti_{an,\ 3\ min}$ catalyst decreases at higher pH.

Table S9. Elemental analyses of Ti content in 0.1 M K_2SO_4 electrolytes before and after they were used for 6 h of FAR at –1.00 V vs RHE. $Ti_{an,\ 3\ min}$ catalysts were used. The mass of dissolved Ti is calculated from the final electrolyte volume (12 mL). To verify that the Ti in the electrolyte is mainly from Ti_{an} and not from the underlying metallic Ti disc substrate, we performed FAR on a polished Ti disc electrode for 6 h. Only a very small amount of Ti (0.14 ppm) could be detected in the electrolyte.

Experiment	pH	Ti in the electrolyte (ppm)	Mass of dissolved Ti (mg)
Ti_{an}, before FAR	2.6	N.D	N.D
Ti_{an}, after 6 h FAR	2.6	8.56	0.103
	3.4	0.45	0.0050
	4.5	0.20	0.0024
	5.8	0.04	0.0005
Ti disc, after 6 h FAR	2.6	0.14	0.0016

N.D.: Not detected.

S3.5. FAR on other metal catalysts

Table S10. Activities of metal catalysts for FAR at –1.00 V vs RHE in 0.1 M K_2SO_4 + 0.5 M HCOOH.

Catalyst	Substrate	Current density (mA/cm^2)	FE_{CH3OH} (%)	j_{CH3OH} (mA/cm^2)	CH_3OH detected (μM)
Fe	Anodized (+0.25 A/cm^2 for 3 min in 0.2 M KCl)	–61	N.D.	N.D.	N.D.
Co		–56	N.D.	N.D.	N.D.
Cu		–216	N.D.	N.D.	N.D.
Zr		–13	N.D.	N.D.	N.D.
Sn		–13	N.D.	N.D.	N.D.
Cr		–100	0.005	–0.007	1.4
Ti		–14	12.6	–1.95	1122
Pd	Polished disc	–95	N.D.	N.D.	N.D.
Cr		–108	0.07	–0.08	22.6
Ti		–87	0.22	–0.12	62.3

N.D.: Not detected.

S4. Active site analysis of Ti_{an} for FAR

S4.1. Electron paramagnetic resonance analysis of Ti_{an}

Table S11. Mass of Ti_{an} (anodized at 1, 2, 3 and 4 min) catalyst powders removed from their disc substrates after they were used for electrocatalytic FAR; their TOV signals were measured using EPR spectroscopy. FAR was conducted for 60 min at –1.00 V vs RHE in 0.1 M K_2SO_4 + 0.5 M HCOOH. Three discs were studied at each anodization time. The TOV signal areas were taken from g =2.1 to g =1.81.

Anodization time (min)	Mass of powder from each substrate (mg)			Mass of accumulated powder from 3 substrates (mg)	TOV EPR signal area (A.U.)	Normalized TOV signal area/mg of powder (A.U.)	j_{CH3OH} (mA/cm^2)
1	0.28	0.19	0.20	0.67	25	37	–0.80
2	0.60	0.76	0.60	1.96	76	39	–1.42
3	1.03	0.98	0.99	3.00	121	40	–1.95
4	1.00	1.17	1.05	3.22	146	45	–2.00
3 (Before FAR)	1.45			1.45	N.D.	N.D.	-

N.D.: Not detected.

S4.2. Cyclic voltammetry and double layer capacitances of Ti_{an}

Table S12. TOV anodic peak areas of Ti_{an} catalysts (anodized at 1, 2, 3 and 4 min) after FAR at –1.00 V vs RHE, measured using cyclic voltammetry. The TOV anodic peak area is taken from –0.85 V to 1.35 V vs RHE. The scan rate was 50 mV/s.

Anodization time/min	Anodic charge densities (mC/cm^2)
1	104 ± 26
2	351 ± 54
3	575 ± 47
4	661 ± 49

S4.3. FAR on control samples

Table S13. Faradaic efficiencies and partial current densities of products detected from electrocatalytic FAR on anatase and rutile TiO_2 dropcast on Ti discs. Experiments were conducted at –1.00 V vs RHE in 0.1 M K_2SO_4 + 0.5 M HCOOH for 60 min.

Sample		CH_3OH	H_2	CH_4	CH_2O	Total
Anatase TiO_2	**FE(%)**	0.18±0.04	90±2	0.021±0.003	N.D.	90±2
	***j*(mA/cm^2)**	–0.05±0.01	–31±6	–0.008±0.002		–31±6
Rutile TiO_2	**FE(%)**	0.03±0.01	90±7	0.02±0.01	0.008±0.006	90±7
	***j*(mA/cm^2)**	–0.05±0.02	–139±38	–0.03±0.02	–0.003±0.002	–139±38

N.D: Not detected.

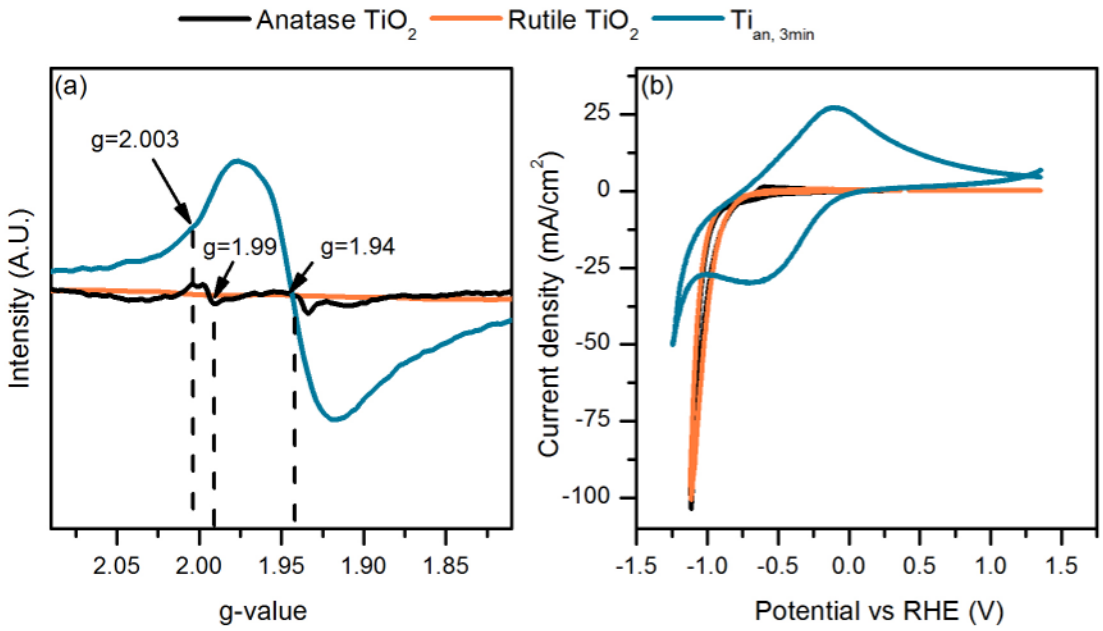

Figure S7. (a) Electron paramagnetic resonance (EPR) spectrum and (b) cyclic voltammogram (CV) of a $Ti_{an,\ 3\ min}$ catalyst, in comparison to those from control anatase and rutile TiO_2 samples. EPR spectroscopy and CV were conducted after 60 min FAR at –1.00 V vs RHE. The peak at g = 1.99 in the EPR spectrum of anatase TiO_2 corresponds to Ti^{3+} centres trapped in the TiO_2 lattice.[23] No Ti^{3+} signals were observed in the EPR spectrum of rutile TiO_2.

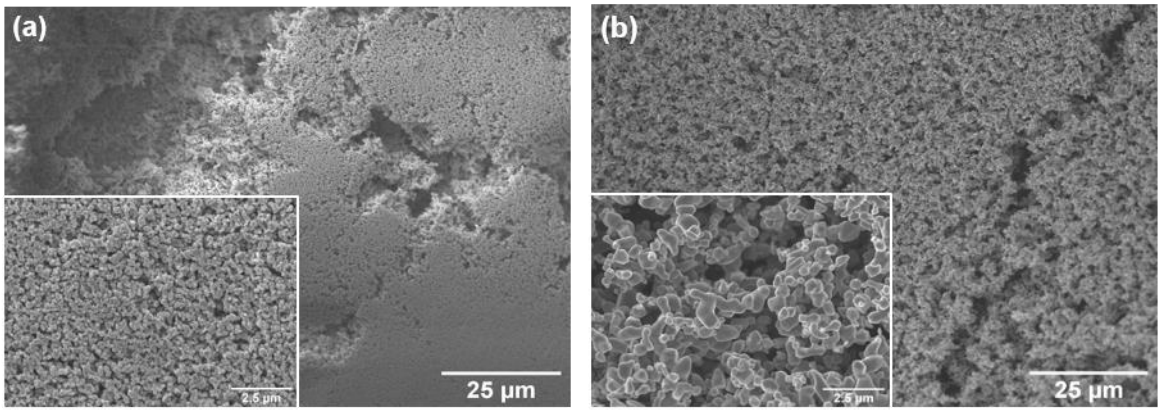

Figure S8. SEM images of crystalline (a) anatase and (b) rutile TiO_2 samples. The insets are the high magnification images of anatase and rutile TiO_2.

S4.4. FAR on Ti_{an} at different anodization times

Table S14. Faradaic efficiencies and partial current densities of products detected from FAR electroreduction on Ti_{an} (anodized for 1, 2, 3 and 4 min). Experiments were conducted at –1.00 V vs RHE for 60 min in 0.1 M K_2SO_4 + 0.5 M HCOOH.

Anodization time/min		CH_3OH	H_2	CH_4	CH_2O	Total
1	**FE(%)**	4.7±1.1	87±1	0.6±0.1	0.08±0.01	92±2
	***j*(mA/cm^2)**	–0.80±0.21	–11.8±0.5	–0.08±0.02	–0.011±0.002	–12.7±0.5
2	**FE(%)**	8.7±1.6	84±6	0.9±0.3	0.11±0.01	94±6
	***j*(mA/cm^2)**	–1.42±0.16	–14±5	–0.16±0.06	–0.019±0.004	–16±5
3	**FE(%)**	12.6±1.8	77±3	1.4±0.3	0.14±0.04	91±4
	***j*(mA/cm^2)**	–1.95±0.20	–12±2	–0.20±0.03	–0.019±0.001	–14±2
4	**FE(%)**	15.2±1.0	70±1	1.7±0.2	0.17±0.02	88±1
	***j*(mA/cm^2)**	–2.00±0.10	–9.8±0.3	–0.23±0.02	–0.023±0.002	–12.0±0.3

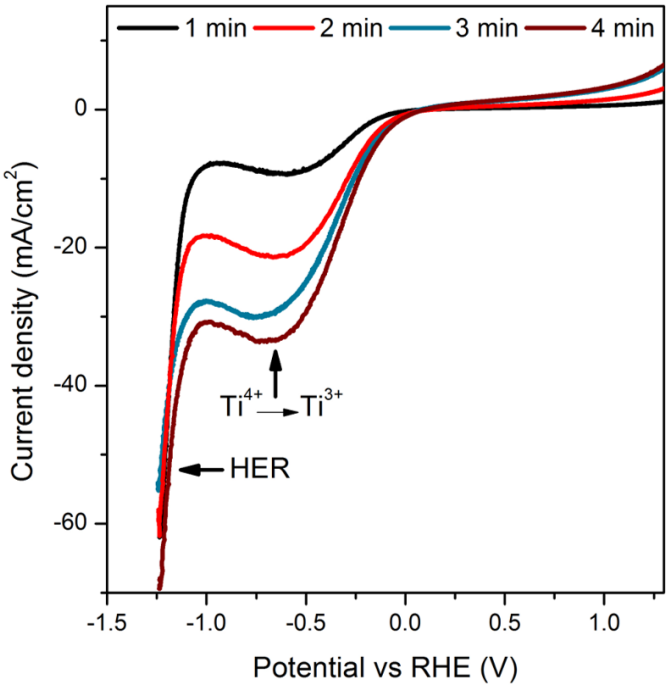

Figure S9. Linear sweep voltammograms of Ti_{an} (anodized for 1, 2, 3 and 4 min). The electrolyte used was 0.1 M K_2SO_4 + 0.5 M HCOOH (pH 2.6). The cathodic peak observed at –0.5 V vs RHE is assigned to the reduction of Ti^{4+} to Ti^{3+}, while the subsequent plunge in current at –1.25 V is assigned largely to the hydrogen evolution reaction.

S5. DFT calculations: tabulated data

S5.1. Adsorption energies

Tables S15a-d. Free energies of adsorption and their contributions for all the possible intermediates involved in the formic acid reduction to methanol at CUS sites. *H is also included. The ZPE, TS_{vib}, and the corresponding ΔG values obtained for the different adsorbates in this study on all the different surface models are listed. $HCOOH_{(l)}$, protons and electrons were used as a reference for all the free energies. All values are in eV.

(a)

TiO_2(110)	ZPE	TS_{vib}	ΔG
*HCOOH	0.93	0.26	–0.44
*H_2COOH	1.26	0.19	1.27
*CHO	0.42	0.20	1.72
*HCOH	0.79	0.19	1.70
*H_2CO	0.78	0.21	–0.09
*CH	0.40	0.04	1.63
*H_2COH	1.16	0.14	1.13
*H_3CO	1.09	0.19	1.12
*O + $CH_3OH_{(l)}$	0.09	0.03	4.37
*H	0.28	0.04	0.09

(b)

TiO_2(120)-BT	ZPE	TS_{vib}	ΔG
*HCOOH	0.93	0.26	–0.29
*H_2COOH	1.26	0.19	1.21
*CHO	0.42	0.20	1.65
*HCOH	0.79	0.19	1.75
*H_2CO	0.78	0.21	–0.10
*CH	0.40	0.04	3.01
*H_2COH	1.16	0.14	1.29
*H_3CO	1.09	0.19	0.92
*O + $CH_3OH_{(l)}$	0.09	0.03	3.94
*H	0.28	0.04	–0.09

(c)

TiO_2(120)-CT	ZPE	TS_{vib}	ΔG
*HCOOH	0.93	0.26	–0.59
*H_2COOH	1.26	0.19	1.57
*CHO	0.42	0.20	1.69
*HCOH	0.79	0.19	1.76
*H_2CO	0.78	0.21	0.03
*CH	0.40	0.04	2.09
*H_2COH	1.16	0.14	1.49
*H_3CO	1.09	0.19	1.24
*O + $CH_3OH_{(l)}$	0.09	0.03	4.54
*H	0.28	0.04	–0.21

(d)

A-TiO_2(101)	ZPE	TS_{vib}	ΔG
*HCOOH	0.93	0.26	–0.64
*H_2COOH	1.26	0.19	1.89
*CHO	0.42	0.20	1.75
*HCOH	0.79	0.19	2.18
*H_2CO	0.78	0.21	0.04
*CH	0.40	0.04	1.77
*H_2COH	1.16	0.14	1.23
*H_3CO	1.09	0.19	1.51
*O + $CH_3OH_{(l)}$	0.09	0.03	4.97
*H	0.28	0.04	0.69

Tables S16a-d. Free energies of adsorption and their contributions for all the possible intermediates involved in the formic acid reduction to methanol at TOV sites. *H is also included. The ZPE, TS_{vib}, and the corresponding ΔG values obtained for the different adsorbates in this study on all the different surface models are listed. $HCOOH_{(l)}$, protons and electrons were used as a reference for all the free energies. All values are in eV.

(a)

TiO_2(110)-O	ZPE	TS_{vib}	ΔG
*HCOOH	0.93	0.26	–0.03
*H_2COOH	1.26	0.19	–1.11
*CHO	0.42	0.20	0.62
*HCOH	0.79	0.19	1.06
*H_2CO	0.78	0.21	–0.99
*CH	0.40	0.04	1.91
*H_2COH	1.16	0.14	0.25
*H_3CO	1.09	0.19	–1.79
*O + $CH_3OH_{(l)}$	0.09	0.03	–1.64
*OH	0.35	0.09	–1.58
*H	0.28	0.04	0.16

(b)

TiO_2(120)-CT-O	ZPE	TS_{vib}	ΔG
*HCOOH	0.93	0.26	0.36
*H_2COOH	1.26	0.19	–0.92
*CHO	0.42	0.20	0.49
*HCOH	0.79	0.19	1.66
*H_2CO	0.78	0.21	0.23
*CH	0.40	0.04	2.56
*H_2COH	1.16	0.14	0.60
*H_3CO	1.09	0.19	–1.38
*O + $CH_3OH_{(l)}$	0.09	0.03	–0.93
*OH	0.35	0.09	–1.17
*H	0.28	0.04	0.56

(c)

TiO_2(120)-BT-O	ZPE	TS_{vib}	ΔG
*HCOOH	0.93	0.26	0.39
*H_2COOH	1.26	0.19	–0.50
*CHO	0.42	0.20	1.17
*HCOH	0.79	0.19	1.87
*H_2CO	0.78	0.21	0.49
*CH	0.40	0.04	2.74
*H_2COH	1.16	0.14	0.80
*H_3CO	1.09	0.19	–1.12
*O + $CH_3OH_{(l)}$	0.09	0.03	–0.82
*OH	0.35	0.09	–0.94
*H	0.28	0.04	0.80

(d)

A-TiO_2(101)-O	ZPE	TS_{vib}	ΔG
*HCOOH	0.93	0.26	–0.22
*H_2COOH	1.26	0.19	–0.32
*CHO	0.42	0.20	0.50
*HCOH	0.79	0.19	0.89
*H_2CO	0.78	0.21	0.30
*CH	0.40	0.04	1.83
*H_2COH	1.16	0.14	0.71
*H_3CO	1.09	0.19	–0.91
*O + $CH_3OH_{(l)}$	0.09	0.03	–1.35
*OH	0.35	0.09	–0.77
*H	0.28	0.04	1.10

S5.2. HER Suppression

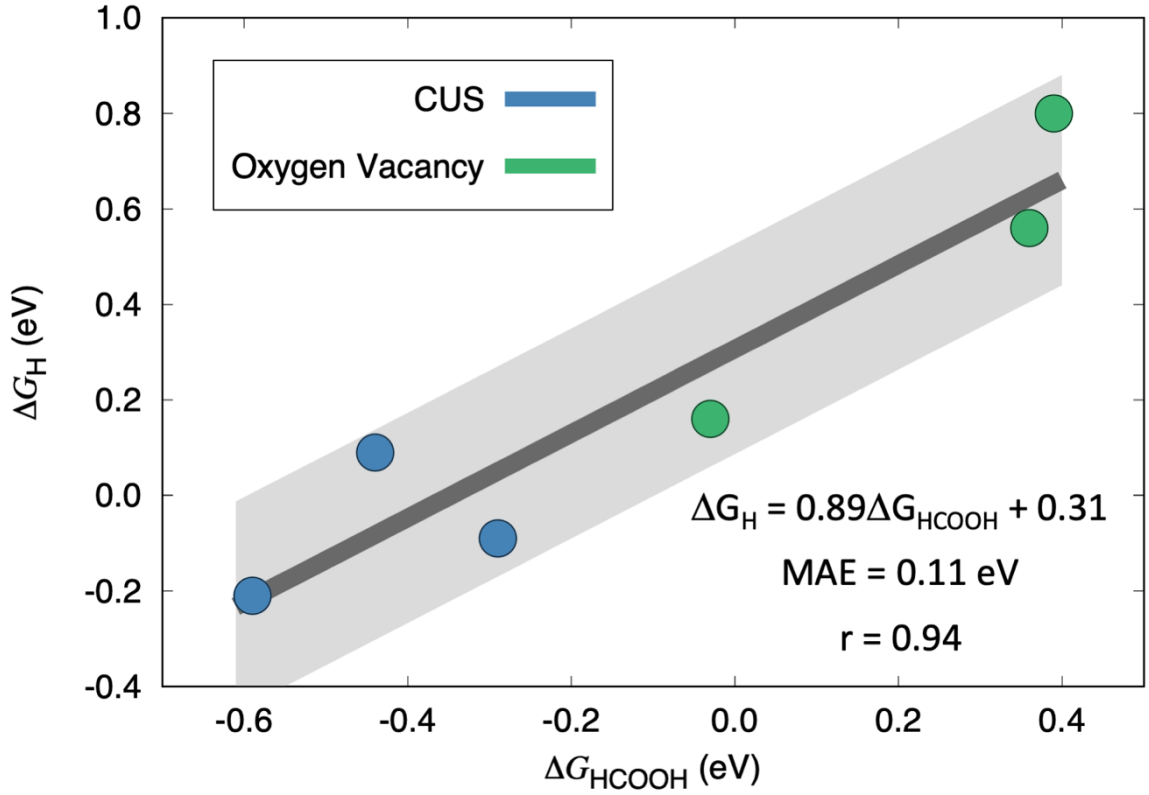

Figure S10. Adsorption-energy scaling relation for *HCOOH and *H. In dark gray we show the linear regression. A light gray zone of ± 2MAE (MAE: mean absolute error) is also shown. The equation, MAE, and Pearson regression coefficient (r) appear at the bottom. The data for CUS sites are shown in blue, while the data for the TOV sites are shown in green.

S6. Electrolysis of proposed FAR intermediates on Ti_{an}

Table S17. Data obtained from the electrocatalytic reduction of possible intermediates for FAR at various potentials using $Ti_{an,\ 3\ min}$ catalysts. Electrolysis were conducted for 60 min. The pH was adjusted to 2.6 using H_2SO_4 for CO, CO_2 and CH_2O experiments. After CH_2O reduction, we detected similar concentrations of CH_3OH and HCOOH. Thus, we conclude that CH_3OH and HCOOH is formed from the Cannizzaro disproportionation of CH_2O. Cannizzaro disproportionation likely occurs due to the higher local pH at the electrode during electrolysis.[3] The current densities observed during CH_2O reduction were attributed to the hydrogen evolution reaction.

Experimental condition	Potential (V vs RHE)	Current density (mA/cm^2)	Methanol detected (μM)	Formate detected (μM)
5 mM CH_2O (nominal concentration added) in 0.1 M K_2SO_4	–0.95	–1.7	59±20	59±12
	–1.00	–1.9	84±19	93±10
	–1.05	–2.4	113±30	119±27
CO in 0.1 M K_2SO_4	–1.00	–2.1	N.D.	N.D.
CO_2 in 0.1 M K_2SO_4	–1.00	–2.6	N.D.	N.D.

N.D- Not detected.

Table S18. CH_2O concentrations measured using the chromotropic acid method before and after CH_2O electrolysis at various potentials using $Ti_{an,\ 3\ min}$ catalysts.

Experimental condition	Potential (V vs RHE)	[CH_2O] (mM)	
		Before electrolysis	After electrolysis
CH_2O in 0.1 M K_2SO_4 (pH 2.6)	–0.95	5.8± 0.5	5.6± 0.5
	–1.00	6.2± 0.2	6.0± 0.2
	–1.05	6.3± 0.3	5.9± 0.5

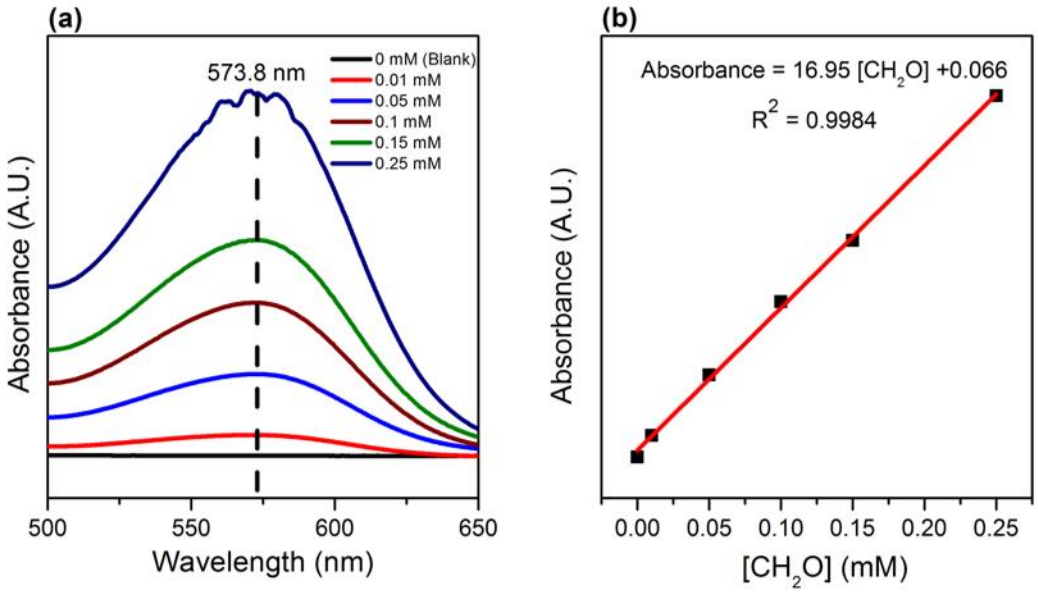

Figure S11. (a) UV-Vis spectra of various CH_2O concentrations measured using the chromotropic acid method. **(b)** Calibration plot of CH_2O concentrations.

S7. Experimental calculations

S7.1. Calculation of FAR equilibrium potential

FAR: $HCOOH + 4H^+ + 4e^- \rightarrow CH_3OH + H_2O$

Based on standard Gibbs free energies of formation at 25 °C and 1 atm,[24]
$\Delta G_{CH3OH\ (l)} = -166.6$ kJ/mol
$\Delta G_{H+} = 0$ kJ/mol
$\Delta G_{H2O\ (l)} = -237.14$ kJ/mol
$\Delta G_{HCOOH\ (l)} = -361.4$ kJ/mol

$\Delta G_{FAR} = (-166.6 - 237.14) - (-361.4) = -42.3$ kJ/mol

$\Delta G = -nFE^o$, where n is the number of electrons utilized for FAR (4 e^-), F is the Faraday constant (96485 C/mol), and E^o is the thermodynamic potential for FAR

$\therefore E^o = \frac{-42.3\times1000}{-(4\times96485)} = +0.11$ V

S7.2. Turnover frequency for CH_3OH production

The average turnover frequency (TOF) for formation of CH_3OH from TOVs was determined using the following formula:

$$\text{TOF} = \frac{No\ of\ moles\ of\ CH_3OH\ formed}{(No\ of\ moles\ of\ TOVs)\times(Time\ of\ reaction)}$$

$HCOOH + 4H^+ + 4e^- \rightarrow CH_3OH + H_2O$

For FAR on a $Ti_{an,\ 3\ min}$ catalyst (area = 0.785 cm^2) in 60 min (3600 s) at –1.0 V vs. RHE, j_{CH3OH} = –1.95 mA/cm^2 (Table S14):

$$\text{Charge} = \frac{1.95\times0.785\times3600}{1000} = 5.51\ \text{C}$$

$$\text{No of moles of electrons for FAR} = \frac{5.51}{96485} = 5.71 \times 10^{-5}\ \text{mol}$$

4 moles of electrons are used to reduce 1 mole of CH_3OH

$$\therefore \text{No of moles of } CH_3OH = \frac{5.71 \times 10^{-5}}{4} = 1.43 \times 10^{-5}\ \text{mol}$$

The population of TOVs was estimated using the charge densities measured from CV.

$Ti^{3+} \rightarrow Ti^{4+} + e^-$

For a $Ti_{an,\ 3\ min}$ catalyst, oxidation peak charge density = 0.575 C/cm^2 (Table S12)

$$\text{No of moles of electrons for TOVs oxidation} = \frac{0.575\times0.785}{96485} = 4.678 \times 10^{-6}\ \text{mol}$$

$$\therefore \text{No of moles of TOVs} = 4.678 \times 10^{-6}\ \text{mol}$$

$$\text{Average TOF} = \frac{1.43 \times 10^{-5}}{(4.678 \times 10^{-6})\times3600} = 8.5 \times 10^{-4}\ s^{-1}$$

S7.3. Cannizzaro disproportionation of CH_2O to CH_3OH and HCOOH

CH_2O is proposed to undergo Cannizzaro disproportionation: $2CH_2O + OH^- \rightarrow HCOO^- + CH_3OH$

Cannizzaro disproportionation of CH_2O is known to occur at pH 3, which is close to our experimental conditions (pH 2.6).[3] $HCOO^-$ is protonated to HCOOH at pH 2.6.

For CH_2O electrolysis at –1.00 V vs RHE:

Concentration of CH_2O ($[CH_2O]$) before electrolysis = 6.2 mM, $[CH_2O]$ after electrolysis = 6.0 mM

Difference in $[CH_2O]$ after electrolysis = 0.2 mM

[HCOOH] before electrolysis (background signal) = 28 μM

[HCOOH] after electrolysis = 121 μM

Difference in [HCOOH] after electrolysis = 93 μM

$[CH_3OH]$ before electrolysis (background signal) = 59 μM

$[CH_3OH]$ after electrolysis = 142 μM

Difference in $[CH_3OH]$ after electrolysis = 84 μM

Sum of CH_3OH and HCOOH concentrations= 93 + 84 = 177 μM (~ 0.2 mM)

The volumes of solutions analyzed using HPLC and HS-GC are the same (1 mL).

Due to an almost 1:1 molar ratio of CH_3OH and HCOOH, it is likely that CH_3OH is formed from the Cannizzaro disproportionation of CH_2O.

S8. Catalytic pathways and computed optimized geometries

The first hydrogenation of *HCOOH can result in the formation of three different intermediates: *H_2COOH, *CHO + H_2O, and *HCOHOH. The free-energy diagrams (Figures S12-S19) show that *H_2COOH is more stable than *CHO + H_2O in all the studied surfaces, both with and without TOVs. *HCOHOH was not included in the diagrams since we did not find any adsorption minimum for this intermediate on any of the model surfaces. In fact, we observed that *HCOHOH generally decomposes into *H and desorbed formic acid.

In Figures S12-S19 we provide the catalytic pathways inspected in this study, based on the energies reported in Tables S15-S16.

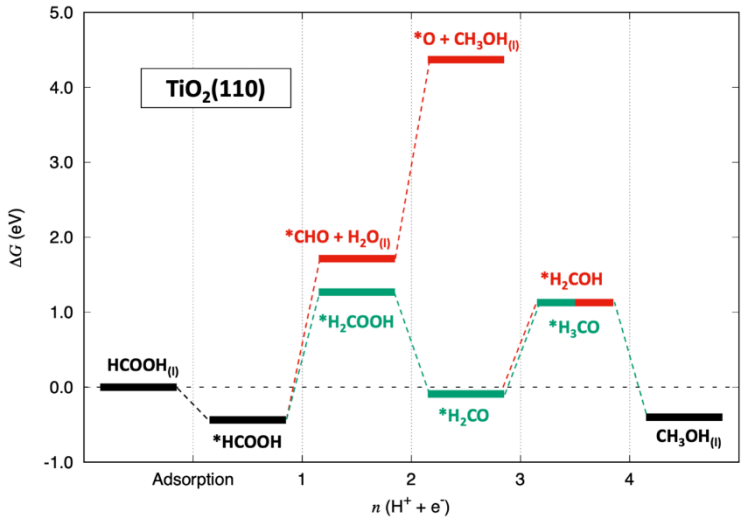

Figure S12. FAR pathways on TiO_2(110) sites. Species common to several pathways are shown in black, the most favorable species in green, and least favorable species in red.

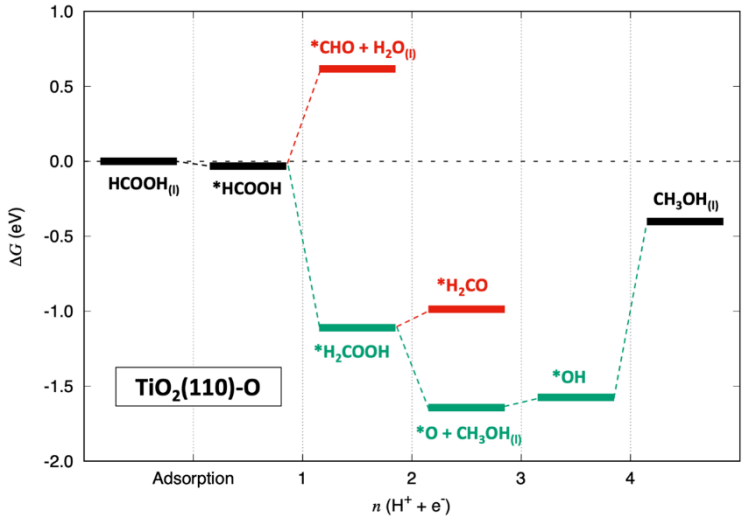

Figure S13. FAR pathways on TiO_2(110)-O sites. Species common to several pathways are shown in black, the most favorable species in green, and least favorable species in red.

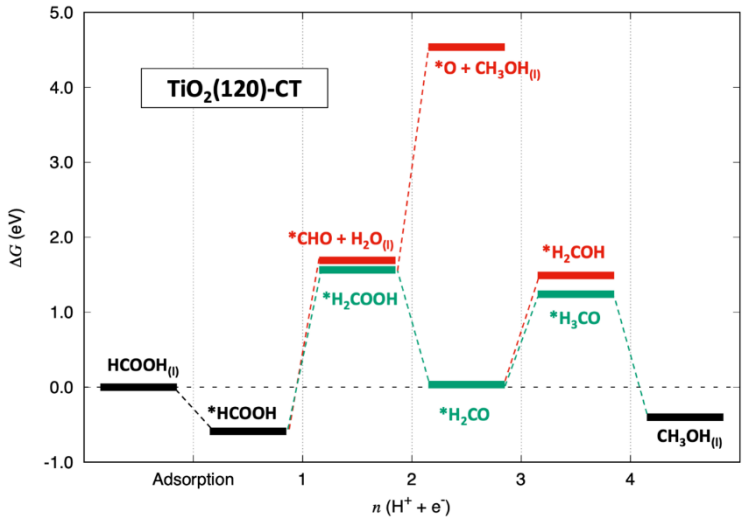

Figure S14. FAR pathways on TiO_2(120)-CT sites. Species common to several pathways are shown in black, the most favorable species in green, and least favorable species in red.

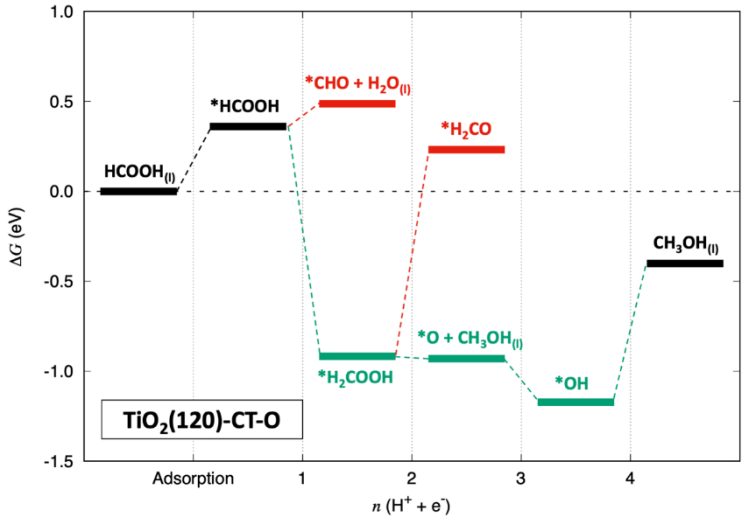

Figure S15. FAR pathways on TiO_2(120)-CT-O sites. Species common to several pathways are shown in black, the most favorable species in green, and least favorable species in red.

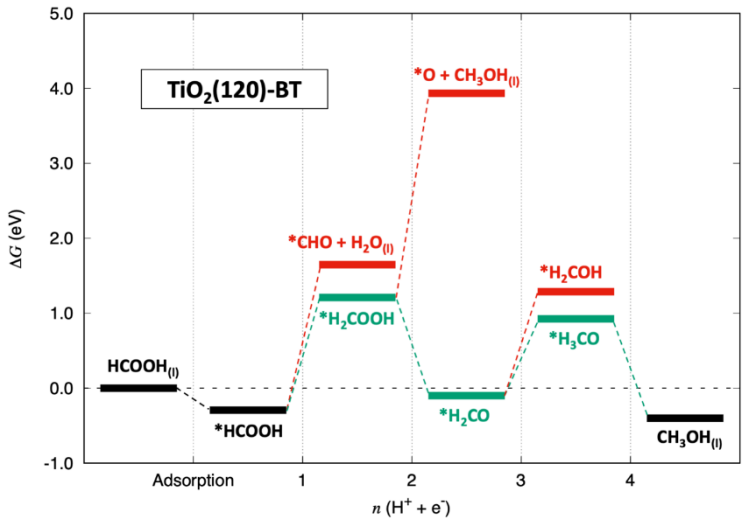

Figure S16. FAR pathways on TiO_2(120)-BT sites. Species common to several pathways are shown in black, the most favorable species in green, and least favorable species in red.

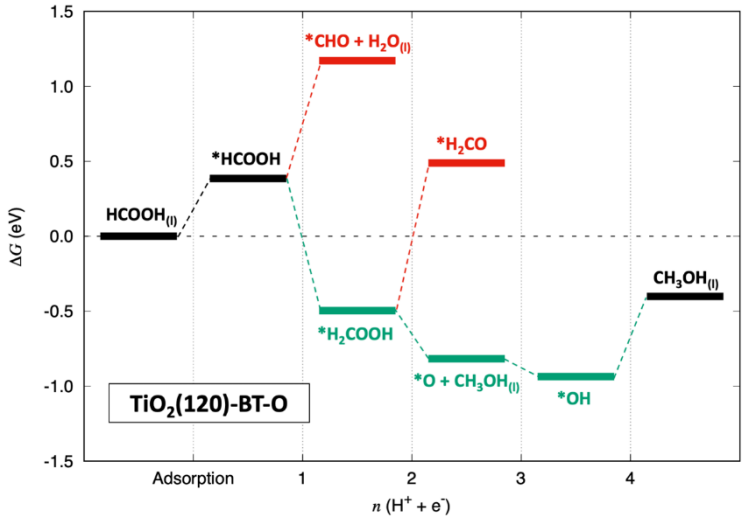

Figure S17. FAR pathways on TiO_2(120)-BT-O sites. Species common to several pathways are shown in black, the most favorable species in green, and least favorable species in red.

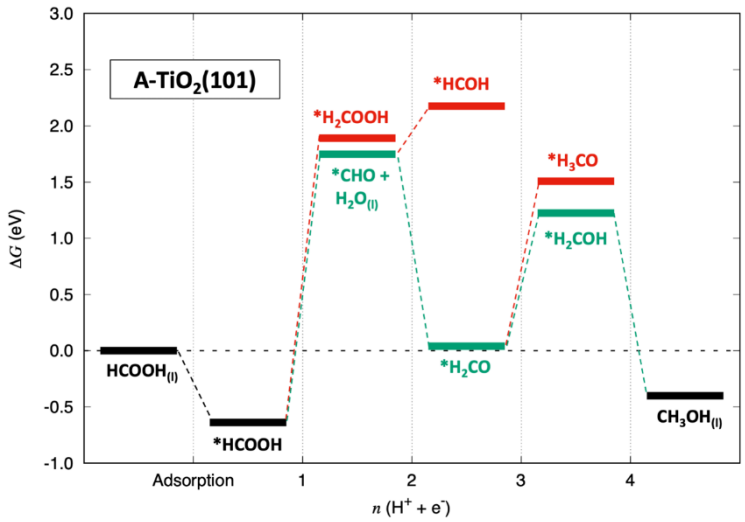

Figure S18. FAR pathways on A-TiO_2(101) sites. Species common to several pathways are shown in black, the most favorable species in green, and least favorable species in red.

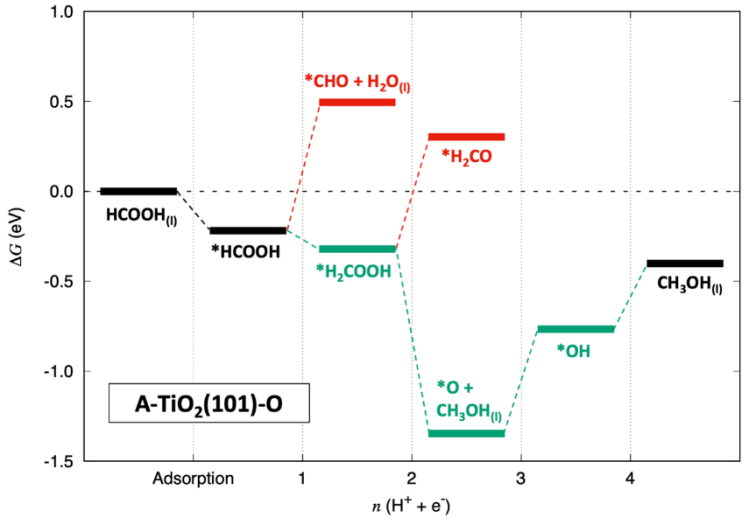

Figure S19. FAR pathways on A-TiO_2(101)-O sites. Species common to several pathways are shown in black, the most favorable species in green, and least favorable species in red.

The coordinates of the optimized geometries for each slab model used in this work are provided in the following pages in the VASP POSCAR format.

TiO_2(110)
1.00000000000000
8.9849996567999995 0.0000000000000000 0.0000000000000000
0.0000000000000000 6.6680169105999996 0.0000000000000000
0.0000000000000000 0.0000000000000000 26.0000000000000000
Ti O
24 48
Selective dynamics
Direct
-0.0000000000000000 0.0000000000000000 0.2607900712831792 T T T
0.3333333333300033 0.0000000000000000 0.2607900712831792 T T T
0.6666666666699967 0.0000000000000000 0.2607900712831792 T T T
0.0000000000000000 0.5000000000000000 0.1282310929999966 F F F
0.3333333333300033 0.5000000000000000 0.1282310929999966 F F F
0.6666666666699967 0.5000000000000000 0.1282310929999966 F F F
-0.0000000000000000 0.5000000000000000 0.3796188237290989 T T T
0.3333333333300033 0.5000000000000000 0.3796188237290989 T T T
0.6666666666699967 0.5000000000000000 0.3796188237290989 T T T
0.1666666666699967 0.0000000000000000 0.1282310929999966 F F F
0.5000000000000000 0.0000000000000000 0.1282310929999966 F F F
0.8333333333300033 0.0000000000000000 0.1282310929999966 F F F
0.1666666666699967 0.0000000000000000 0.3918456323554846 T T T
0.5000000000000000 0.0000000000000000 0.3918456323554846 T T T
0.8333333333300033 0.0000000000000000 0.3918456323554846 T T T
0.1666666666699967 0.5000000000000000 0.0000000000000000 F F F
0.5000000000000000 0.5000000000000000 0.0000000000000000 F F F
0.8333333333300033 0.5000000000000000 0.0000000000000000 F F F
0.1666666666699967 0.5000000000000000 0.2545641396850890 T T T
0.5000000000000000 0.5000000000000000 0.2545641396850890 T T T
0.8333333333300033 0.5000000000000000 0.2545641396850890 T T T
0.0000000000000000 0.0000000000000000 0.0000000000000000 F F F
0.3333333333300033 0.0000000000000000 0.0000000000000000 F F F
0.6666666666699967 0.0000000000000000 0.0000000000000000 F F F
0.1666666666699967 0.3046543600000007 0.1282310929999966 F F F
0.5000000000000000 0.3046543600000007 0.1282310929999966 F F F
0.8333333333300033 0.3046543600000007 0.1282310929999966 F F F
0.1666666666699967 0.3133159194297828 0.3912737905739085 T T T
0.5000000000000000 0.3133159194297828 0.3912737905739085 T T T
0.8333333333300033 0.3133159194297828 0.3912737905739085 T T T
0.1666666666699967 0.8046543600000007 0.0000000000000000 F F F
0.5000000000000000 0.8046543600000007 0.0000000000000000 F F F
0.8333333333300033 0.8046543600000007 0.0000000000000000 F F F
0.1666666666699967 0.8015105855347157 0.2572283095351653 T T T
0.5000000000000000 0.8015105855347157 0.2572283095351653 T T T
0.8333333333300033 0.8015105855347157 0.2572283095351653 T T T
0.1666666666699967 0.6953456399999993 0.1282310929999966 F F F
0.5000000000000000 0.6953456399999993 0.1282310929999966 F F F
0.8333333333300033 0.6953456399999993 0.1282310929999966 F F F
0.1666666666699967 0.6866840805702170 0.3912737905739085 T T T
0.5000000000000000 0.6866840805702170 0.3912737905739085 T T T
0.8333333333300033 0.6866840805702170 0.3912737905739085 T T T
0.1666666666699967 0.1953456399999993 0.0000000000000000 F F F
0.5000000000000000 0.1953456399999993 0.0000000000000000 F F F
0.8333333333300033 0.1953456399999993 0.0000000000000000 F F F
0.1666666666699967 0.1984894144652848 0.2572283095351653 T T T
0.5000000000000000 0.1984894144652848 0.2572283095351653 T T T
0.8333333333300033 0.1984894144652848 0.2572283095351653 T T T
0.0000000000000000 0.0000000000000000 0.0781323240000020 F F F
0.3333333333300033 0.0000000000000000 0.0781323240000020 F F F
0.6666666666699967 0.0000000000000000 0.0781323240000020 F F F
-0.0000000000000000 0.0000000000000000 0.3351540548242291 T T T
0.3333333333300033 0.0000000000000000 0.3351540548242291 T T T
0.6666666666699967 0.0000000000000000 0.3351540548242291 T T T
-0.0000000000000000 0.5000000000000000 0.2072183169431961 T T T
0.3333333333300033 0.5000000000000000 0.2072183169431961 T T T
0.6666666666699967 0.5000000000000000 0.2072183169431961 T T T
0.0000000000000000 0.0000000000000000 0.1783298699999989 F F F
0.3333333333300033 0.0000000000000000 0.1783298699999989 F F F
0.6666666666699967 0.0000000000000000 0.1783298699999989 F F F
-0.0000000000000000 0.0000000000000000 0.4351021240667713 T T T
0.3333333333300033 0.0000000000000000 0.4351021240667713 T T T
0.6666666666699967 0.0000000000000000 0.4351021240667713 T T T
0.0000000000000000 0.5000000000000000 0.0500987730000020 F F F
0.3333333333300033 0.5000000000000000 0.0500987730000020 F F F
0.6666666666699967 0.5000000000000000 0.0500987730000020 F F F
-0.0000000000000000 0.5000000000000000 0.3071124558058780 T T T
0.3333333333300033 0.5000000000000000 0.3071124558058780 T T T
0.6666666666699967 0.5000000000000000 0.3071124558058780 T T T
0.0000000000000000 0.5000000000000000 0.9499012229999977 F F F
0.3333333333300033 0.5000000000000000 0.9499012229999977 F F F
0.6666666666699967 0.5000000000000000 0.9499012229999977 F F F

A-TiO_2(101)
1.00000000000000
10.4802742004000002 0.0000000000000000 0.0000000000000000
0.0000000000000000 7.7779998780000001 0.0000000000000000
0.0000000000000000 0.0000000000000000 28.0000000000000000
Ti O
32 64
Selective dynamics
Direct
0.2065483929999985 0.2500000000000000 0.1934642049999979 F F F
0.2065483929999985 0.7500000000000000 0.1934642049999979 F F F
0.3427173489937766 0.2500000000000000 0.3233355407680694 T T T
0.3427173489937766 0.7500000000000000 0.3233355407680694 T T T
0.4846613029010779 0.2500000000000000 0.4557106602606070 T T T
0.4846613029010780 0.7500000000000000 0.4557106602606070 T T T
0.8532742260000035 0.0000000000000000 0.0967321019999972 F F F
0.8532742260000035 0.5000000000000000 0.0967321019999972 F F F
0.9909731150000027 0.0000000000000000 0.2257082460000035 F F F
0.9909731150000027 0.5000000000000000 0.2257082460000035 F F F
0.1244524171549186 0.0000000000000000 0.3529934158325181 T T T
0.1244524171549186 0.5000000000000000 0.3529934158325181 T T T
0.2579398776152889 0.0000000000000000 0.4792606789195057 T T T

0.2579398776152889 0.5000000000000000 0.4792606789195057 T T T
0.5688495039999992 0.0000000000000000 0.0644880760000035 F F F
0.5688495039999992 0.5000000000000000 0.0644880760000035 F F F
0.7065483929999985 0.0000000000000000 0.1934642049999979 F F F
0.7065483929999985 0.5000000000000000 0.1934642049999979 F F F
0.8427172899937754 0.0000000000000000 0.3233355407680694 T T T
0.8427172899937754 0.5000000000000000 0.3233355407680694 T T T
0.9846613629010829 0.0000000000000000 0.4557106602606070 T T T
0.9846613629010829 0.5000000000000000 0.4557106602606070 T T T
0.3532741960000010 0.2500000000000000 0.0967321019999972 F F F
0.3532741960000010 0.7500000000000000 0.0967321019999972 F F F
0.4909731449999981 0.2500000000000000 0.2257082460000035 F F F
0.4909731449999981 0.7500000000000000 0.2257082460000035 F F F
0.6244523871549229 0.2500000000000000 0.3529934158325181 T T T
0.6244523871549229 0.7500000000000000 0.3529934158325181 T T T
0.7579398186152878 0.2500000000000000 0.4792606789195057 T T T
0.7579398186152878 0.7500000000000000 0.4792606789195057 T T T
0.0688499999999976 0.2500000000000000 0.0644899999999993 F F F
0.0688499999999976 0.7500000000000000 0.0644899999999993 F F F
0.1745316089999989 0.2500000000000000 0.1234669910000008 F F F
0.1745316089999989 0.7500000000000000 0.1234669910000008 F F F
0.3122305269999970 0.2500000000000000 0.2524431350000000 F F F
0.3122305269999970 0.7500000000000000 0.2524431350000000 F F F
0.4501873610673087 0.2500000000000000 0.3820814900212765 T T T
0.4501873610673087 0.7500000000000000 0.3820814900212765 T T T
0.5987824771933588 0.2500000000000000 0.5090622707548003 T T T
0.5987824771933588 0.7500000000000000 0.5090622707548003 T T T
0.8901068569999993 0.2500000000000000 0.0912229640000035 F F F
0.8901068569999993 0.7500000000000000 0.0912229640000035 F F F
0.0278058419999994 0.2500000000000000 0.2201990929999980 F F F
0.0278058419999994 0.7500000000000000 0.2201990929999980 F F F
0.1631085365419702 0.2500000000000000 0.3485164974503860 T T T
0.1631085365419702 0.7500000000000000 0.3485164974503860 T T T
0.3068250647638940 0.2500000000000000 0.4859143652917746 T T T
0.3068250647638940 0.7500000000000000 0.4859143652917746 T T T
0.0320167880000000 0.0000000000000000 0.0699972139999971 F F F
0.0320167880000000 0.5000000000000000 0.0699972139999971 F F F
0.1697157170000025 0.0000000000000000 0.1989733280000010 F F F
0.1697157170000025 0.5000000000000000 0.1989733280000010 F F F
0.3058976416808436 -0.0000000000000000 0.3278429842061035 T T T
0.3058976416808436 0.5000000000000000 0.3278429842061035 T T T
0.4448685204429828 -0.0000000000000000 0.4578031389154402 T T T
0.4448685204429828 0.5000000000000000 0.4578031389154402 T T T
0.7475920320000000 0.0000000000000000 0.0377531760000025 F F F
0.7475920320000000 0.5000000000000000 0.0377531760000025 F F F
0.8852909800000006 0.0000000000000000 0.1667293160000014 F F F
0.8852909800000006 0.5000000000000000 0.1667293160000014 F F F
0.0215955299828127 0.0000000000000000 0.2954649913992957 T T T
0.0215955299828127 0.5000000000000000 0.2954649913992957 T T T
0.1644062599447616 -0.0000000000000000 0.4229215550560427 T T T
0.1644062599447616 0.5000000000000000 0.4229215550560427 T T T
0.6745316390000013 0.0000000000000000 0.1234669910000008 F F F
0.6745316390000013 0.5000000000000000 0.1234669910000008 F F F
0.8122305269999970 0.0000000000000000 0.2524431350000000 F F F
0.8122305269999970 0.5000000000000000 0.2524431350000000 F F F
0.9501873310673133 0.0000000000000000 0.3820814900212765 T T T
0.9501873310673133 0.5000000000000000 0.3820814900212765 T T T
0.0987824471933561 -0.0000000000000000 0.5090622707548003 T T T
0.0987824471933561 0.5000000000000000 0.5090622707548003 T T T
0.3901068870000017 0.0000000000000000 0.0912229640000035 F F F
0.3901068870000017 0.5000000000000000 0.0912229640000035 F F F
0.5278058649999977 0.0000000000000000 0.2201990929999980 F F F
0.5278058649999977 0.5000000000000000 0.2201990929999980 F F F
0.6631085965419680 0.0000000000000000 0.3485164974503860 T T T
0.6631085965419680 0.5000000000000000 0.3485164974503860 T T T
0.8068250947638892 -0.0000000000000000 0.4859143652917746 T T T
0.8068250947638892 0.5000000000000000 0.4859143652917746 T T T
0.5320167539999971 0.2500000000000000 0.0699972139999971 F F F
0.5320167539999971 0.7500000000000000 0.0699972139999971 F F F
0.6697157030000014 0.2500000000000000 0.1989733280000010 F F F
0.6697157030000014 0.7500000000000000 0.1989733280000010 F F F
0.8058976116808410 0.2500000000000000 0.3278429842061035 T T T
0.8058976116808410 0.7500000000000000 0.3278429842061035 T T T
0.9448684314429860 0.2500000000000000 0.4578031389154402 T T T
0.9448684314429860 0.7500000000000000 0.4578031389154402 T T T
0.3852909510000018 0.2500000000000000 0.1667293160000014 F F F
0.3852909510000018 0.7500000000000000 0.1667293160000014 F F F
0.2475919869999998 0.2500000000000000 0.0377531829999995 F F F
0.2475919869999998 0.7500000000000000 0.0377531829999995 F F F
0.5215954519828135 0.2500000000000000 0.2954649913992957 T T T
0.5215954519828135 0.7500000000000000 0.2954649913992957 T T T
0.6644062749447593 0.2500000000000000 0.4229215550560427 T T T
0.6644062749447593 0.7500000000000000 0.4229215550560427 T T T

TiO_2(120)-CT

1.00000000000000
10.5430603027000007 0.0000000000000000 0.0000000000000000
0.0000000000000000 8.9849996566999994 0.0000000000000000
0.0000000000000000 0.0000000000000000 29.0861206054999997
Ti O
39 78
Selective dynamics
Direct
0.0000000000000000 0.0000000000000000 0.3624773619999999 F F F
0.0000000000000000 0.3333333429999996 0.3624773619999999 F F F
0.0000000000000000 0.6666666870000029 0.3624773619999999 F F F
0.2000000029999995 0.0000000000000000 0.2174864409999984 F F F
0.2000000029999995 0.3333333429999996 0.2174864409999984 F F F
0.2000000029999995 0.6666666870000029 0.2174864409999984 F F F
0.1921070460591643 -0.0000000000000000 0.5785403126817833 T T T
0.1921070460591643 0.3333333429999996 0.5785403126817833 T T T
0.1921070460591643 0.6666666870000029 0.5785403126817833 T T T
0.8000000119999982 0.0000000000000000 0.1449909509999969 F F F
0.8000000119999982 0.3333333429999996 0.1449909509999969 F F F
0.8000000119999982 0.6666666870000029 0.1449909509999969 F F F
0.7962796961005532 -0.0000000000000000 0.5031368076207411 T T T
0.7962796961005532 0.3333333429999996 0.5031368076207411 T T T
0.7962796961005532 0.6666666870000029 0.5031368076207411 T T T
0.6000000239999963 0.0000000000000000 0.2899819020000010 F F F
0.6000000239999963 0.3333333429999996 0.2899819020000010 F F F
0.6000000239999963 0.6666666870000029 0.2899819020000010 F F F
0.4044382593574338 0.0000000000000000 0.4395090649306257 T T T
0.4044382593574338 0.3333333429999996 0.4395090649306257 T T T
0.4044382593574338 0.6666666870000029 0.4395090649306257 T T T
0.1020937633327484 0.1666666719999981 0.4710231122834402 T T T
0.1020937633327484 0.5000000000000000 0.4710231122834402 T T T
0.1020937633327484 0.8333333129999971 0.4710231122834402 T T T
0.3000000119999982 0.1666666719999981 0.3262296320000004 F F F
0.3000000119999982 0.5000000000000000 0.3262296320000004 F F F
0.3000000119999982 0.8333333129999971 0.3262296320000004 F F F
0.8999999759999966 0.1666666719999981 0.2537341709999978 F F F
0.8999999759999966 0.5000000000000000 0.2537341709999978 F F F
0.8999999759999966 0.8333333129999971 0.2537341709999978 F F F
0.6962354674594750 0.1666666719999981 0.3973770966184393 T T T
0.6962354674594750 0.5000000000000000 0.3973770966184393 T T T
0.6962354674594750 0.8333333129999971 0.3973770966184393 T T T
0.5000000000000000 0.1666666719999981 0.1812386810000035 F F F
0.5000000000000000 0.5000000000000000 0.1812386810000035 F F F
0.5000000000000000 0.8333333129999971 0.1812386810000035 F F F
0.5011977714674070 0.1666666719999981 0.5511335811515042 T T T
0.5011977714674070 0.5000000000000000 0.5511335811515042 T T T
0.5011977714674070 0.8333333129999971 0.5511335811515042 T T T
0.2821543211303802 0.1666666719999981 0.4496785411078291 T T T
0.2821543211303802 0.5000000000000000 0.4496785411078291 T T T
0.2821543211303802 0.8333333129999971 0.4496785411078291 T T T
0.4827926159999976 0.1666666719999981 0.3041435780000015 F F F
0.4827926159999976 0.5000000000000000 0.3041435780000015 F F F
0.4827926159999976 0.8333333129999971 0.3041435780000015 F F F
0.0827926400000010 0.1666666719999981 0.2316480880000000 F F F
0.0827926400000010 0.5000000000000000 0.2316480880000000 F F F
0.0827926400000010 0.8333333129999971 0.2316480880000000 F F F
0.1002409862854206 0.1666666719999981 0.6005091719739730 T T T
0.1002409862854206 0.5000000000000000 0.6005091719739730 T T T
0.1002409862854206 0.8333333129999971 0.6005091719739730 T T T
0.8821350387154232 0.1666666719999981 0.3768199428874975 T T T
0.8821350387154232 0.5000000000000000 0.3768199428874975 T T T
0.8821350387154232 0.8333333129999971 0.3768199428874975 T T T
0.6827926039999994 0.1666666719999981 0.1591526119999997 F F F
0.6827926039999994 0.5000000000000000 0.1591526119999997 F F F
0.6827926039999994 0.8333333129999971 0.1591526119999997 F F F
0.6973573562649136 0.1666666719999981 0.5259842732051350 T T T
0.6973573562649136 0.5000000000000000 0.5259842732051350 T T T
0.6973573562649136 0.8333333129999971 0.5259842732051350 T T T
0.9172073599999990 0.1666666719999981 0.1308292599999987 F F F
0.9172073599999990 0.5000000000000000 0.1308292599999987 F F F
0.9172073599999990 0.8333333129999971 0.1308292599999987 F F F
0.9216962975501899 0.1666666719999981 0.4974752764952646 T T T
0.9216962975501899 0.5000000000000000 0.4974752764952646 T T T
0.9216962975501899 0.8333333129999971 0.4974752764952646 T T T
0.1172074079999987 0.1666666719999981 0.3483156859999994 F F F
0.1172074079999987 0.5000000000000000 0.3483156859999994 F F F
0.1172074079999987 0.8333333129999971 0.3483156859999994 F F F
0.7172073130000030 0.1666666719999981 0.2758202249999968 F F F
0.7172073130000030 0.5000000000000000 0.2758202249999968 F F F
0.7172073130000030 0.8333333129999971 0.2758202249999968 F F F
0.5203687574834706 0.1666666719999981 0.4208090252742405 T T T
0.5203687574834706 0.5000000000000000 0.4208090252742405 T T T
0.5203687574834706 0.8333333129999971 0.4208090252742405 T T T
0.3172073360000027 0.1666666719999981 0.2033247350000025 F F F
0.3172073360000027 0.5000000000000000 0.2033247350000025 F F F
0.3172073360000027 0.8333333129999971 0.2033247350000025 F F F
0.3223133096931612 0.1666666719999981 0.5720572955639349 T T T
0.3223133096931612 0.5000000000000000 0.5720572955639349 T T T
0.3223133096931612 0.8333333129999971 0.5720572955639349 T T T
0.0579560115184227 -0.0000000000000000 0.4296360571932812 T T T
0.0579560115184227 0.3333333429999996 0.4296360571932812 T T T
0.0579560115184227 0.6666666870000029 0.4296360571932812 T T T
0.2609308660000025 0.0000000000000000 0.2837446030000024 F F F
0.2609308660000025 0.3333333429999996 0.2837446030000024 F F F
0.2609308660000025 0.6666666870000029 0.2837446030000024 F F F
0.8609308599999963 0.0000000000000000 0.2112491279999986 F F F
0.8609308599999963 0.3333333429999996 0.2112491279999986 F F F
0.8609308599999963 0.6666666870000029 0.2112491279999986 F F F
0.6623330800199384 -0.0000000000000000 0.3568471336138694 T T T
0.6623330800199384 0.3333333429999996 0.3568471336138694 T T T
0.6623330800199384 0.6666666870000029 0.3568471336138694 T T T
0.4609308839999997 0.0000000000000000 0.1387536670000031 F F F
0.4609308839999997 0.3333333429999996 0.1387536670000031 F F F
0.4609308839999997 0.6666666870000029 0.1387536670000031 F F F
0.4638068770269656 0.0000000000000000 0.5011139618916026 T T T
0.4638068770269656 0.3333333429999996 0.5011139618916026 T T T
0.4638068770269656 0.6666666870000029 0.5011139618916026 T T T
0.1388668776993872 -0.0000000000000000 0.5141222509638022 T T T
0.1388668776993872 0.3333333429999996 0.5141222509638022 T T T
0.1388668776993872 0.6666666870000029 0.5141222509638022 T T T
0.3390691279999984 0.0000000000000000 0.3687146600000020 F F F
0.3390691279999984 0.3333333429999996 0.3687146600000020 F F F
0.3390691279999984 0.6666666870000029 0.3687146600000020 F F F
0.9390691520000018 0.0000000000000000 0.2962191700000005 F F F
0.9390691520000018 0.3333333429999996 0.2962191700000005 F F F
0.9390691520000018 0.6666666870000029 0.2962191700000005 F F F

0.74003945055321870 -0.00000000000000000 0.44140595111887996 T T T
0.74003945055321870 0.33333334299999960 0.44140595111887996 T T T
0.74003945055321870 0.66666668700000290 0.44140595111887996 T T T
0.53906911600000030 0.00000000000000000 0.22372372400000270 F F F
0.53906911600000030 0.33333334299999960 0.22372372400000270 F F F
0.53906911600000030 0.66666668700000290 0.22372372400000270 F F F
0.54482168397732200 -0.00000000000000000 0.58613763612814500 T T T
0.54482168397732200 0.33333334299999960 0.58613763612814500 T T T
0.54482168397732200 0.66666668700000290 0.58613763612814500 T T T

TiO_2(120)-BT

1.00000000000000
10.54306030270000070 0.00000000000000000 0.00000000000000000
0.00000000000000000 8.98499965669999940 0.00000000000000000
0.00000000000000000 0.00000000000000000 29.08612060549999970
Ti O
39 78
Selective dynamics
Direct
0.00331232384083040 0.00000000000000000 0.36285420426416330 T T T
0.00331232384083040 0.33333334299999960 0.36285420426416330 T T T
0.00331232384083040 0.66666668700000290 0.36285420426416330 T T T
0.20000000299999950 0.00000000000000000 0.21748644009999840 F F F
0.20000000299999950 0.33333334299999960 0.21748644009999840 F F F
0.20000000299999950 0.66666668700000290 0.21748644009999840 F F F
0.80000001199999820 0.00000000000000000 0.14499095099999690 F F F
0.80000001199999820 0.33333334299999960 0.14499095099999690 F F F
0.80000001199999820 0.66666668700000290 0.14499095099999690 F F F
0.60331339154366110 0.00000000000000000 0.29309740218245160 T T T
0.60331339154366110 0.33333334299999960 0.29309740218245160 T T T
0.60331339154366110 0.66666668700000290 0.29309740218245160 T T T
0.40000000599999910 0.00000000000000000 0.07249547499999660 F F F
0.40000000599999910 0.33333334299999960 0.07249547499999660 F F F
0.40000000599999910 0.66666668700000290 0.07249547499999660 F F F
0.40110801775187940 -0.00000000000000000 0.43074723150331660 T T T
0.40110801775187940 0.33333334299999960 0.43074723150331660 T T T
0.40110801775187940 0.66666668700000290 0.43074723150331660 T T T
0.10000000099999800 0.16666667199999810 0.10874322099999740 F F F
0.10000000099999800 0.50000000000000000 0.10874322099999740 F F F
0.10000000099999800 0.83333331299999710 0.10874322099999740 F F F
0.11265259223259960 0.16666667199999810 0.47253814379559014 T T T
0.11265259223259960 0.50000000000000000 0.47253814379559014 T T T
0.11265259223259960 0.83333331299999710 0.47253814379559014 T T T
0.30021623460387330 0.16666667199999810 0.32433210681467370 T T T
0.30021623460387330 0.50000000000000000 0.32433210681467370 T T T
0.30021623460387330 0.83333331299999710 0.32433210681467370 T T T
0.89999997599999660 0.16666667199999810 0.25373417099999780 F F F
0.89999997599999660 0.50000000000000000 0.25373417099999780 F F F
0.89999997599999660 0.83333331299999710 0.25373417099999780 F F F
0.69999998800000180 0.16666667199999810 0.03624774499999720 F F F
0.69999998800000180 0.50000000000000000 0.03624774499999720 F F F
0.69999998800000180 0.83333331299999710 0.03624774499999720 F F F
0.71045133949168660 0.16666667199999810 0.40239948561358150 T T T
0.71045133949168660 0.50000000000000000 0.40239948561358150 T T T
0.71045133949168660 0.83333331299999710 0.40239948561358150 T T T
0.50000000000000000 0.16666667199999810 0.18123868100000350 F F F
0.50000000000000000 0.50000000000000000 0.18123868100000350 F F F
0.50000000000000000 0.83333331299999710 0.18123868100000350 F F F
0.28279262800000280 0.16666667199999810 0.08665714400000010 F F F
0.28279262800000280 0.50000000000000000 0.08665714400000010 F F F
0.28279262800000280 0.83333331299999710 0.08665714400000010 F F F
0.29540646730050260 0.16666667199999810 0.45753128791771290 T T T
0.29540646730050250 0.50000000000000000 0.45753128791771290 T T T
0.29540646730050260 0.83333331299999710 0.45753128791771290 T T T
0.47928490953573680 0.16666667199999810 0.30440265376210680 T T T
0.47928490953573680 0.50000000000000000 0.30440265376210680 T T T
0.47928490953573680 0.83333331299999710 0.30440265376210680 T T T
0.08279264000000100 0.16666667199999810 0.23164808800000000 F F F
0.08279264000000100 0.50000000000000000 0.23164808800000000 F F F
0.08279264000000100 0.83333331299999710 0.23164808800000000 F F F
0.88732607311393160 0.16666667199999810 0.37543442351609540 T T T
0.88732607311393160 0.50000000000000000 0.37543442351609540 T T T
0.88732607311393160 0.83333331299999710 0.37543442351609540 T T T
0.68279260399999940 0.16666667199999810 0.15915261199999970 F F F
0.68279260399999940 0.50000000000000000 0.15915261199999970 F F F
0.68279260399999940 0.83333331299999710 0.15915261199999970 F F F
0.91720735999999900 0.16666667199999810 0.13082925999999870 F F F
0.91720735999999900 0.50000000000000000 0.13082925999999870 F F F
0.91720735999999900 0.83333331299999710 0.13082925999999870 F F F
0.12322092564947700 0.16666667199999810 0.34813147160977600 T T T
0.12322092564947700 0.50000000000000000 0.34813147160977600 T T T
0.12322092564947690 0.83333331299999710 0.34813147160977600 T T T
0.71714467758930780 0.16666667199999810 0.27706908435974500 T T T
0.71714467758930780 0.50000000000000000 0.27706908435974500 T T T
0.71714467758930780 0.83333331299999710 0.27706908435974500 T T T
0.51720738400000240 0.16666667199999810 0.05833379900000320 F F F
0.51720738400000240 0.50000000000000000 0.05833379900000320 F F F
0.51720738400000240 0.83333331299999710 0.05833379900000320 F F F
0.51795174662180690 0.16666667199999810 0.42861795160673780 T T T
0.51795174662180690 0.50000000000000000 0.42861795160673780 T T T
0.51795174662180690 0.83333331299999710 0.42861795160673780 T T T
0.31720733600000270 0.16666667199999810 0.20332473500000250 F F F
0.31720733600000270 0.50000000000000000 0.20332473500000250 F F F
0.31720733600000270 0.83333331299999710 0.20332473500000250 F F F
0.06093086700000330 0.00000000000000000 0.06625818500000240 F F F
0.06093086700000330 0.33333334299999960 0.06625818500000240 F F F
0.06093086700000330 0.66666668700000290 0.06625818500000240 F F F
0.06418404041901130 0.00000000000000000 0.42753602678432530 T T T
0.06418404041901130 0.33333334299999960 0.42753602678432530 T T T
0.06418404041901130 0.66666668700000290 0.42753602678432530 T T T
0.26148207213809900 -0.00000000000000000 0.28468810327649840 T T T
0.26148207213809900 0.33333334299999960 0.28468810327649840 T T T
0.26148207213809900 0.66666668700000290 0.28468810327649840 T T T
0.86093085999999630 0.00000000000000000 0.21124912799999860 F F F
0.86093085999999630 0.33333334299999960 0.21124912799999860 F F F
0.86093085999999630 0.66666668700000290 0.21124912799999860 F F F
0.65360658257547640 0.00000000000000000 0.35715604072653150 T T T
0.65360658257547640 0.33333334299999960 0.35715604072653150 T T T
0.65360658257547640 0.66666668700000290 0.35715604072653150 T T T
0.46093088399999970 0.00000000000000000 0.13875366700000310 F F F
0.46093088399999970 0.33333334299999960 0.13875366700000310 F F F
0.46093088399999970 0.66666668700000290 0.13875366700000310 F F F
0.13906912499999890 0.00000000000000000 0.15122823400000130 F F F
0.13906912499999890 0.33333334299999960 0.15122823400000130 F F F
0.13906912499999890 0.66666668700000290 0.15122823400000130 F F F
0.10536248496517460 -0.00000000000000000 0.51187206758447970 T T T
0.10536248496517460 0.33333334299999960 0.51187206758447970 T T T
0.10536248496517460 0.66666668700000290 0.51187206758447970 T T T
0.34147412335827680 -0.00000000000000000 0.37049385849633250 T T T
0.34147412335827680 0.33333334299999960 0.37049385849633250 T T T
0.34147412335827680 0.66666668700000290 0.37049385849633250 T T T
0.94159424056822160 -0.00000000000000000 0.29588268027422170 T T T
0.94159424056822160 0.33333334299999960 0.29588268027422170 T T T
0.94159424056822160 0.66666668700000290 0.29588268027422170 T T T
0.73906910400000210 0.00000000000000000 0.07873277400000230 F F F
0.73906910400000210 0.33333334299999960 0.07873277400000230 F F F
0.73906910400000210 0.66666668700000290 0.07873277400000230 F F F
0.74438310054764610 -0.00000000000000000 0.43959634683255820 T T T
0.74438310054764610 0.33333334299999960 0.43959634683255820 T T T
0.74438310054764610 0.66666668700000290 0.43959634683255820 T T T
0.53906911600000030 0.00000000000000000 0.22372372400000270 F F F
0.53906911600000030 0.33333334299999960 0.22372372400000270 F F F
0.53906911600000030 0.66666668700000290 0.22372372400000270 F F F
0.66092997799999860 0.00000000000000000 0.99375999000000090 F F F
0.66092997799999860 0.33333334299999960 0.99375999000000090 F F F
0.66092997799999860 0.66666668700000290 0.99375999000000090 F F F

S9. References

(1) Low, Q. H.; Loo, N. W. X.; Calle-Vallejo, F.; Yeo, B. S. Enhanced Electroreduction of Carbon Dioxide to Methanol Using Zinc Dendrites Pulse-Deposited on Silver Foam. *Angew. Chem., Int. Ed.* **2019**, *58* (8), 2256–2260.

(2) Shariati-Rad, M.; Irandoust, M.; Mozaffarinia, N. Response Surface Methodology in Spectrophotometric Determination of Formaldehyde Using Chromotropic Acid. *Anal. Bioanal. Chem. Res.* **2016**, *3* (2), 149–157.

(3) Birdja, Y. Y.; Koper, M. T. M. The Importance of Cannizzaro-Type Reactions during Electrocatalytic Reduction of Carbon Dioxide. *J. Am. Chem. Soc.* **2017**, *139* (5), 2030–2034.

(4) Strunk, J.; Vining, W. C.; Bell, A. T. A Study of Oxygen Vacancy Formation and Annihilation in Submonolayer Coverages of TiO_2 Dispersed on MCM-48. *J. Phys. Chem. C* **2010**, *114* (40), 16937–16945.

(5) Fu, G.; Zhou, P.; Zhao, M.; Zhu, W.; Yan, S.; Yu, T.; Zou, Z. Carbon Coating Stabilized Ti^{3+}-Doped TiO_2 for Photocatalytic Hydrogen Generation under Visible Light Irradiation. *Dalton Trans.* **2015**, *44* (28), 12812–12817.

(6) Kresse, G.; Furthmüller, J. Efficient Iterative Schemes for Ab Initio Total-Energy Calculations Using a Plane-Wave Basis Set. *Phys. Rev. B* **1996**, *54* (16), 11169–11186.

(7) Perdew, J. P.; Yang, W.; Burke, K.; Yang, Z.; Gross, E. K. U.; Scheffler, M.; Scuseria, G. E.; Henderson, T. M.; Zhang, I. Y.; Ruzsinszky, A.; Peng, H.; Sun, J.; Trushin, E.; Görling, A. Understanding Band Gaps of Solids in Generalized Kohn-Sham Theory. *Proc. Natl. Acad. Sci.* **2017**, *114* (11), 2801–2806.

(8) Kresse, G.; Joubert, D. From Ultrasoft Pseudopotentials to the Projector Augmented-Wave Method. *Phys. Rev. B* **1999**, *59* (3), 1758–1775.

(9) Xu, Z.; Rossmeisl, J.; Kitchin, J. R. A Linear Response DFT+U Study of Trends in the Oxygen Evolution Activity of Transition Metal Rutile Dioxides. *J. Phys. Chem. C* **2015**, *119* (9), 4827–4833.

(10) Monkhorst, H. J.; Pack, J. D. Special Points for Brillonin-Zone Integrations. *Phys. Rev. B* **2019**, *13* (12), 5188–5192.

(11) Siahrostami, S.; Vojvodic, A. Influence of Adsorbed Water on the Oxygen Evolution Reaction on Oxides. *J. Phys. Chem. C* **2015**, *119* (2), 1032–1037.

(12) Mathew, K.; Sundararaman, R.; Letchworth-Weaver, K.; Arias, T. A.; Hennig, R. G. Implicit Solvation Model for Density-Functional Study of Nanocrystal Surfaces and Reaction Pathways. *J. Chem. Phys.* **2014**, *140* (8), 084106.

(13) Briquet, L. G. V.; Sarwar, M.; Mugo, J.; Jones, G.; Calle-Vallejo, F. A New Type of Scaling Relations to Assess the Accuracy of Computational Predictions of Catalytic Activities Applied to the Oxygen Evolution Reaction. *ChemCatChem* **2017**, *9* (7), 1261–1268.

(14) Nørskov, J. K.; Rossmeisl, J.; Logadottir, A.; Lindqvist, L.; Kitchin, J. R.; Bligaard, T.; Jónsson, H. Origin of the Overpotential for Oxygen Reduction at a Fuel-Cell Cathode. *J. Phys. Chem. B* **2004**, *108* (46), 17886–17892.

(15) Granda-Marulanda, L. P.; Rendón-Calle, A.; Builes, S.; Illas, F.; Koper, M. T. M.; Calle-Vallejo, F. A Semiempirical Method to Detect and Correct DFT-Based Gas-Phase Errors and Its Application in Electrocatalysis. *ACS Catal.* **2020**, *10* (12), 6900–6907.

(16) Calle-Vallejo, F.; Koper, M. T. M. Theoretical Considerations on the Electroreduction of CO to C_2 Species on Cu(100) Electrodes. *Angew. Chem., Int. Ed.* **2013**, *52* (28), 7282–7285.

(17) Pouilleau, J.; Devilliers, D.; Garrido, F.; Durand-Vidal, S.; Mahé, E. Structure and Composition of Passive Titanium Oxide Films. *Mater. Sci. Eng., B* **1997**, *47* (3), 235–243.

(18) Walle, L. E.; Borg, A.; Johansson, E. M. J.; Plogmaker, S.; Rensmo, H.; Uvdal, P.; Sandell, A. Mixed Dissociative and Molecular Water Adsorption on Anatase TiO_2(101). *J. Phys. Chem. C* **2011**, *115* (19), 9545–9550.

(19) Kato, K.; Xin, Y.; Shirai, T. Structural-Controlled Synthesis of Highly Efficient Visible Light TiO_2 Photocatalyst via One-Step Single-Mode Microwave Assisted Reaction. *Sci. Rep.* **2019**, *9* (1), 1–9.

(20) Zhang, Z.; Hedhili, M. N.; Zhu, H.; Wang, P. Electrochemical Reduction Induced Self-Doping of Ti^{3+} for Efficient Water Splitting Performance on TiO_2 Based Photoelectrodes. *Phys. Chem. Chem. Phys.* **2013**, *15* (37), 15637–15644.

(21) Qiu, M.; Tian, Y.; Chen, Z.; Yang, Z.; Li, W.; Wang, K.; Wang, L.; Wang, K.; Zhang, W. Synthesis of Ti^{3+} Self-Doped TiO_2 Nanocrystals Based on Le Chatelier's Principle and Their Application in Solar Light Photocatalysis. *RSC Adv.* **2016**, *6* (78), 74376–74383.

(22) Balachandran, U.; Eror, N. G. Raman Spectra of Titanium Dioxide. *J. Solid State Chem.* **1982**, *42* (3), 276–282.

(23) Chiesa, M.; Paganini, M. C.; Livraghi, S.; Giamello, E. Charge Trapping in TiO_2 Polymorphs as Seen by Electron Paramagnetic Resonance Spectroscopy. *Phys. Chem. Chem. Phys.* **2013**, *15* (24), 9435–9447.

(24) Dean, J. A. Section 6: Thermodynamic Properties. In *Lange's Handbook of Chemistry.*; Dean, J. A., Lange, N. A., Eds.; McGraw-Hill: Knoxville, **1999**; pp 6.1-6.147.